Heat exchange in a mechanically stirred granular bed : application to the SIMSAN sodium carbonation process

SCK.CEN

Waste and Clean-up Division

Department BR3 Decommissioning

715/05-03b

Pierre-François BIARD

Eleve-ingénieur deuxième année

ENSCR

Eric CANTREL

SCK•CEN

D&D Waste Management

Training period from the 2nd of May to the 31st of August 2005 in Mol (BELGIUM)

Table of Contents

Foreword

The Belgian Nuclear Research Centre (SCK•CEN) is a Foundation of Public Utility (FPU), with a legal status according to private law, under the supervision of the Belgian Federal Minister in charge of energy. SCK•CEN has about 600 employees present on two sites: Brussels for the registered office and Mol, near Antwerpen, for the operational office. It was created in 1952 in order to give the Belgian academic and industrial world access to the worldwide development of nuclear energy.

By research and development, training, communication and services, SCK•CEN contributes to:

- nuclear safety and radiation protection,
- medical and industrial applications of radioisotopes,
- the backend of the nuclear fuel cycle,
- long term storage,
- dismantling.

Since 1991, research programs on societal acceptance of nuclear energy and ethic programs have been introduced.

Many different installations or laboratories are present on the site of Mol such as three nuclear reactors, an underground research laboratory at a depth of 225 meters and several others facilities. These available know-how and infrastructures are also used for services to industry and for training of employees.

My trainee ship occurred in the Belgium Reactor 3 (BR3) in the Radioactive Waste and Site Restoration Division. BR3 was the first prototype of the pressurized water reactors (PWR's) brought into service in Europe in 1962. SCK•CEN could not demonstrate that the integrity of the pressure vessel was assured in all circumstances; consequently, it was shut down in 1987. Then, it was selected as a European pilot project for the demonstration of decommissioning of NPP (Nuclear Power Plant): optimization of dismantling and decontamination techniques, realistic assessment of costs, development of techniques for minimization of waste and implementation of evacuation route.

I would wish particularly to thank my supervisor, Eric CANTREL for his assistance and his advices; John SEGHERS to have allowed me to join him for different visits of factories; and Pierre VALENDUC for his sympathy. I also wish to thank Jean-Michel BEC, Walter SANCHEZ and Yoann DESCAS for their friendly company.

Introduction

Metallic sodium has been widely used in the fields of research, development and exploitation of fast breeder reactors as a coolant. Despite it reacts violently with substances such as water and other oxidants, it has been selected for its good thermal properties, its low viscosity and its low melting point (97°C). This sodium became activated (formation of radioisotopes: ^{22}Na, ^{24}Na, and ^{25}Na) and/or contaminated by radioactive compounds (^{3}H, ^{60}Co, ^{55}Fe) depending on the nature of the experiments. As a result of experiments, 90 litres of contaminated sodium must be treated in SCK•CEN. More important amounts of contaminated sodium are present in other countries. For example, 5500 tones of sodium have to be treated in France due to the exploitation of Superphenix. Although it reacts more violently than the pure sodium, NaK (alloy of sodium and potassium) has been also used as a coolant with the advantage of being liquid at the ambient temperature.

Several processes have been developed to treat these alkali metals. Thus, CEA (Commissariat à l'Energie Atomique), the French nuclear research centre, has developed a process called NOAH in which the contaminated sodium reacts with water to form hydrogen and sodium hydroxide which could be integrated in limited content in the composition of concrete (125 to 150 kg of sodium for 1 m^3 of concrete). This process could convert 5 tones per day of sodium. It is actually under operation in Scotland in the site of Dounreay. The drawback of NOAH is that the final product is not really stable and must be handled with care before being integrated in a concrete. Moreover, the conversion is highly exothermic and generates important amounts of hydrogen which is an explosive combustive gas.

SCK•CEN has carried out several experiments involving molten sodium as coolant. Some years ago, SCK•CEN started to look for an efficient and safe technology for this waste resulting in a waste form which is ready for further conditioning. SCK•CEN looks after the development of a simple and safe batch process to meet safety and disposal requirements.

The proposed process is a two-step conversion where the metallic sodium is firstly dispersed in an inert matrix of sodium carbonate. At the end, the product is pure sodium carbonate which can be dispersed in a concrete, a ceramic or a glass matrix. No hydrogen is formed during the process. As the reactions are exothermic, total and instantaneous in the operating conditions, the conversion rate of the process is limited by the heat transfer rate between a coolant and the packed bed where the conversion occurs. The feasibility has been tested at laboratory scale. Then, a semi-industrial pilot installation has been constructed to demonstrate the process with non-active sodium for batches of 1 to 5 kg of sodium.

The aim of this trainee ship was to find a suitable model for the heat transfer in the process, calculate it and to present different possible optimisations.

1 The SimSan Project

1.1 Principle and objectives

The main idea is to convert, without any production of hydrogen, the metallic contaminated sodium in a sodium carbonate powder (soda ash) which is a stable product. In order to achieve this objective, the sodium is firstly heated above the melting point temperature (97°C) and dispersed in a matrix of sodium carbonate to realize a coating. Although other granular materials could have been used (silica, sand, alumina…), the same substance than the final product has been chosen expecting a re-use of it.

In a first stage, the sodium is oxidized by gaseous O_2 at a temperature range of 270-300°C. Two ways are possible leading respectively to sodium oxide and sodium peroxide:

$4\ Na + O_2\ (g) \rightarrow 2\ Na_2O$ (1) $\Delta_rH°(1) = -845.8$ kJ/mol of O_2 (300°C)

$2\ Na + O_2\ (g) \rightarrow Na_2O_2$ (2) $\Delta_rH°(2) = -516.3$ kJ/mol of O_2 (300°C)

Finally, these two products are converted in sodium carbonate by injecting CO_2:

$Na_2O + CO_2\ (g) \rightarrow Na_2CO_3$ (3) $\Delta_rH°(3) = -316.1$ kJ/mol of CO_2 (300°C)

$2\ Na_2O_2 + 2\ CO_2\ (g) \rightarrow 2\ Na_2CO_3 + O_2\ (g)$ (4) $\Delta_rH°(4) = -222.6$ kJ/mol of CO_2 (300°C)

The total balance is:

$2\ Na + CO_2\ (g) + \frac{1}{2}\ O_2\ (g) \rightarrow Na_2CO_3$ $\Delta_rH°(tot) = -369.5$ kJ/mol of Na (300°C)

These reactions are instantaneous and total at the operating temperature (270 to 300°C). At the end, all the sodium is converted in sodium carbonate. This product could be used several times over and finally immobilized in a concrete, a ceramic or a glass matrix

This conversion is carried out in a vessel with a double mantle. In the double mantle, a coolant is flowing in order to control the temperature within the bed of powder as the reactions are highly exothermic. This bed is mechanically agitated in order to realize the coating and to increase the mass and heat transfer rates by mixing effects.

The coating allows to have a high sodium surface area targeting:

- the complete conversion of the metallic sodium by the absence of clusters
- a large contact surface area between the gaseous reagent and the sodium
- a good control of the chemical reactions and associated heat production
- an efficient heat transfer in avoiding hot spots.

1.2 Description of the pilot installation

The flowsheet and technical drawings are present in appendix 1.

The pilot installation is settled in a highly ventilated confinement.

The metallic sodium coating, the oxidation and carbonation are carried out in the reactor MSR. This reactor has a double mantle where the coolant (specifications in appendix 2, table 6) circulates at approximately 70 L/min which is the maximum flow achievable with the thermoregulators circulating pumps. The double mantle and the cover of the reactor are thermally insulated by rock wool. The vessel wall is in stainless steel 316.

A gas circulation line is present downstream and upstream of the reactor. This gas circulation line includes a gas feeding unit and a resistance to warm up the gases before their entrance in the reactor. Upstream it, a gas buffer tank equipped with a rupture disk (3 bar) is present in order to protect the installation from overpressure and gas backflow. An O_2/CO_2 analyzer is used to detect the amounts of O_2 and CO_2 upstream. A sodium melting tank in series with an injection line heated by means of a heated wire allows to melt the sodium outside the reactor and then to inject it under safe conditions (flow of an inert gas). Moreover two thermoregulators are used: to warm up and cool down the reactor for the first one (THR 1) and to cool down the gas at the exhaust and the stirring device for the second one (THR 2). Two solids tanks which are present above and below the reactor allow respectively to load the fresh carbonate and to remove the final one.

Various technologies are available to stir a bed (moving, fluidized or agitated bed). In a previous project called Sands, SCK•CEN tried to convert the sodium using a fluidized bed. Due to the difficulty to inject the sodium, this project has been given up. Then a mechanically agitated bed in vertical position has been chosen for the SimSan Project. This technology avoids the problem of the injection as a coating is firstly realised. Moreover, it allows keeping a good heat transfer rate [1]. The vertical position favours a good circulation of the gases all over the radial position.

Various devices of mixing also exist. The main ones are the scrapper, the paddle-type blade and the helicoïdal screw. In the pilot, paddle type blades turning at 800 rpm have been used in addition to scrappers turning at 15 rpm. Small amounts of sodium (1 to 5 kg) have been totally converted. As this device was used at a high velocity, it consumed a lot of energy and caused attrition of the particles (appendix 5). Moreover, the paddle type blades are not the best mean to mix the bed as it can ensure that the totality of the bed is agitated (radially and axially). On the contrary, scrappers allow increasing the heat transfer rates ensuring a good renewal of the particles at the wall [18]. Consequently, this device has been recently replaced by a helicoïdal screw operating at 165 rpm which generates a convective mixing effect.

More information about the installation is presented in the technical report [33].

1.3 The different steps of the process and the operating conditions

The process is operated batchwise. Each batch is carried out according to the following sequence: the matrix is firstly dried. The sodium is cleaned under an inert gas flow, introduced in the tank, melted and injected in the reactor vessel. The coating is realised under agitation.

The reactor is warm up to the conversion temperature and, the oxidation and carbonation are achieved. This last step is described below and the others one in the technical reports [33,34].

Once the reactor blend has reached the reaction temperature between 270°C and 300°C, the oxidation is initiated. O_2 is injected in addition of an inert gas (Argon in the pilot but other gases as Nitrogen or Helium could be considered) previously used during the drying of the matrix and the coating. The gases are injected at 200°C. A smaller quantity of CO_2 is injected simultaneously to limit Na_2O_2 accumulation which is an unstable potentially explosive oxidant. The oxygen flow rate is slowly raised until the working flow is reached. When a breakthrough of O_2 is observed in the outlet, the O_2 flow rate is slowly decreased whereas the CO_2 flow rate is increased. During the conversion, the inlet coolant temperature is adjusted to reach steady state conditions. The total gas flow rate must not exceed the minimum of fluidization in the vessel (appendix 2, table 7). When the nominal injection CO_2 concentration is obtained at the exhaust, which means that no carbonation still occurs, the experiment is stopped and the reactor is cooled down under inert gas flow. In order to re-use the final product and to add new sodium, the vessel is not full of powder and consequently there is a gas phase at the top. The process operates at the atmospheric pressure. The amount of Na introduced is equal to 10 % of the amount of Na_2CO_3 in mass [33].

The other operating and technical conditions which are useful in the topic of heat transfer are all presented in appendix 2.

2 Heat transfers in the pilot

Basic notions in heat transfer useful in this study are presented in appendix 3.

2.1 Introduction

As a coolant flows in the double mantle, we can consider that forced convection occurs there. Between the double mantle and the vessel, heat is exchanged by conduction through the inner wall. As the reactions are exothermic, heat is produced in the bed and must be evacuated. How this heat produced is transferred within the bed and between the bed and the wall? The heat exchange should increase thanks to the mechanical agitation. Moreover, as the top of the vessel is filled by the carrier gas, we should consider convection in it. As the gases in the pilot arrives at the bottom at 200°C despite the bed is at 300°C, heat is also transferred from the bed to the gases. The last point to take into consideration is the heat loss. According to the calculations presented in appendix 4, the heat transferred from the double mantle to the air in vicinity of the reactor amounts to approximately 300 W.

Thus, it may be possible to modelise the heat transfer between the coolant and the bed considering three radial resistances in series: in the double mantle where heat is transferred by convection, in the wall of the vessel where heat is transferred by conduction and in the packed bed. The two first resistances could be calculated with confidence using the classical

correlations (appendix 3) at the contrary of the last one which required a bibliographical research.

Nevertheless, it may be possible to see if some phenomena can be neglected in the bed. Whereas Argon was used in the pilot as a carrier gas, the final choice has not been done yet. Consequently, in this study, three gases will be compared: Argon, Nitrogen and Helium.

2.2 Evaluation of the heat transferred from the bed to the gas flowing through

In the pilot, the gas mixture arrives at the bottom of the bed at a temperature lower than the bed temperature. Consequently, heat is transferred from the bed to the gas leading to a heat loss in the vessel by the gas flow. In the literature, it is possible to find correlations to evaluate it [27, 28, 29]. Nevertheless, considering that the gas arrives at 200°C and leaves the vessel at the most at 300°C (the temperature of the bed), the maximal heat flux exchanged between the bed and the gas (Q_{gas}^{max}) could be calculated and compared with the heat produced during the experiments ($Q_{produced}$). $Q_{produced}$ is the total heat evacuated in the process.

$$Q_{gas}^{max} = F \cdot Cp_{gas} \cdot \Delta\theta = F \cdot Cp_{gas} \cdot (300 - 200) \quad (1)$$

F: mass flow rate of the carrier gas ($kg.s^{-1}$)
Cp: heat capacity of the carrier gas ($J.kg^{-1}.K^{-1}$)

Taking into account that O_2 and CO_2 react instantaneously, we consider that heat is transferred only to the carrier gas (Ar). The flow rates of the gases are taken a little below their respective minimum of fluidization (appendix 2, table 8). $Q_{produced}$ is approximately equals to 2500 W according to the first experiments carried out.

	Ar	N_2	He
Cp ($J.kg^{-1}.K^{-1}$)	520	1057	5197
Mass flow rate ($kg.s^{-1}$)	2,5E-04	2,1E-04	3,0E-04
Q_{gas} (W)	1,3E+01	2,3E+01	1,5E+02
$Q_{gas}/Q_{produced}$ (%)	0,5	0,9	6,2

Table 1: Evaluation of the heat transferred from the bed to the gas

It appears finally that the ratio $Q_{gas}/Q_{produced}$ is low (table 1) using Argon and Nitrogen. Due to the high heat capacity of Helium, the heat cleared by the gas becomes more important and should be taken into account.

Consequently, in the actual pilot, the heat evacuated by the flow of Argon could be neglected in comparison with the heat evacuated by the double mantle.

2.3 Evaluation of the heat transferred by convection at the top of the vessel

As the vessel is not full of powder, there is a gas phase at the top of it. Consequently, heat could be transferred by convection in forced regime.

For the three gases (Ar, He, N_2), the regime is clearly laminar and the Reynolds's number don't exceed 34 taking the flow rates at the minimum of fluidization. As the temperature of the gas phase is unknown in the interval 200-300°C, the calculation is done at 200 °C $\left(T_{gas}^{min}\right)$ in order to be conservative. The Nusselt number is estimated thanks to the correlation (7) of the appendix 3. The convection coefficient in the top of the vessel (h) is deduced from the Nusselt number. A temperature of 300 °C for the wall (T_{wall}) is assumed in order to estimate the maximal heat transfer rate by convection between the gas and the wall (Q_{conv}^{max}).

$$Q_{conv}^{max} = h \cdot A_{gas} \cdot \left(T_{wall} - T_{gas}^{min}\right) = h \cdot A_{gas} \cdot (300 - 200) \qquad (2)$$

A_{gas}: heat exchange area between the gas phase and the inner wall=0,179 m^2

	Ar (g)	N_2 (g)	He (g)
μ/μ_p	1,190	1,130	1,136
Flow rate ($NL.min^{-1}$)	8	10	100
Re	25,3	26,7	34,0
Nu	5,6	5,8	6,3
h ($W.m^{-2}.K^{-1}$)	0,4	0,6	3,4
Q_{conv} (W)	7	10	61
Q_{conv}/Q_{prod} (%)	0,3	0,4	2,4

Table 2: Evaluation of the convection coefficient in the gas phase

The ratios between the maximal heat rates dissipated by convection over the heat produced are low. Consequently, this means of heat transfer could be neglected in the calculations.

2.4 The thermodynamic issue of the conversion

Two ways are possible to oxidise the sodium:

- in sodium peroxide (Na_2O_2): $\Delta_r G°_{Na->Na2O2}$ = -194,4 kJ/mol Na at 300°C
- in sodium oxide (Na_2O): $\Delta_r G°_{Na->Na2O}$ = -170,2 kJ/mol Na at 300°C

Taking into account the global reaction, the two ways are thermodynamically equivalent with a $\Delta_r H°$ which is equal to -369.5 kJ per mol of Na. The reactions are fast and total in the operating conditions. There is no kinetic control of the reactions. According to the value of $\Delta_r G°$ the way via the sodium peroxide is in majority at 300°C.

During the processing, the oxidation and carbonation are not achieved simultaneously: at the beginning, O_2 is introduced in majority. The amounts of sodium oxide and peroxide converted are unknown. Moreover, during the oxidation step, a small amount of CO_2 is introduced in order to avoid the accumulation of sodium peroxide which is unstable and explosive. The conversion of the sodium peroxide previously formed generates O_2 which could also reacts and the amount of peroxide and oxide converted are unknown. Consequently it is impossible to evaluate with a good accuracy the heat produced by the reaction.

Nevertheless, this value could be framed during the oxidation step between minimal and maximal values considering respectively that all the O_2 introduced reacts by the peroxide way and by the oxide way.

In order to evaluate with a better accuracy the heat produced, it would be interesting to estimate the ratio of sodium peroxide over sodium oxide produced in the operating conditions. The idea is to convert a little amount of sodium but with only an oxygen flow. The amount of O_2 necessary is deduced when an O_2 breakthrough is detected. Knowing approximately the amount of O_2 necessary to convert a given amount of sodium, we can deduce the quantity of sodium converted by each path and then estimate the heat produced.

2.5 Conclusion

According to the analysis of the different ways of heat transfer in the bed, it would be possible to consider that the heat exchanged occurs between the bed and the wall in contact with it, then by conduction in the wall and finally by convection in the double mantle. All these phenomena are in series.

Consequently, the difficulty lies in the expression of the heat transfer coefficient between the wall and the bed mechanically agitated where an exothermic reaction occurs. The heat transfer coefficient is called the “wall-to-bed” heat transfer coefficient. A bibliographical research is necessary to express it.

3 The “wall-to-bed” heat transfer

Various researches in several databases (SCIFinder, Compendex, Inspec, Science Citation Index and Google Scholar) and Internet have been performed. According to the results found, it appears that few authors have studied the topic of heat transfer in mechanically agitated beds contrary to heat transfer in fluidized beds.

3.1 Introduction

The researches concerning the heat exchanges in this technology have begun in the sixties. The results given by the precursors are very limited because they are not really founded theoretically [9]. Some of them propose empirical correlations.

The correlating equations of Otake and Tone are based on the concept that in heat transfer to a mixed bed, two processes take place: heat transfer as in a fixed bed by conduction, and the transport of heat due to the mixing of the particles [2, 3]. The drawback of the correlations proposed by the authors is the complexity of their applications in practical cases.

Garner, Botterill and Ross consider the mechanically mixed bed as a transitional stage between a fixed and fluidized bed [4]. Their derivation of a theoretical relation for the calculation of the heat transfer coefficient is based on the assumption that there is only a point contact between a particle and the wall, which does not allow the heat transfer between the bed and the wall. All the heat exchanged between them must be therefore transferred by the gas filling the voids. This assumption is verified experimentally by Botterill and co-workers [5]. The drawback of the model proposed by them is due to the somewhat unsuitable definition of the radial efficiency of the mixer.

The influence of convection and conduction of heat in the gaseous phase is dealt with by Dunskij [6, 7]. He shows by a theoretical reasoning that a decrease in the rate of heat transfer by these mechanisms can lead to such a slow heating of the particles in contact with the wall that their temperature will practically not change even over a prolonged period of contact (N-B: In these studies, no reaction occurs, therefore the only heat source comes from the wall). For shorter periods of contact of particles with the wall, the driving force for heat transfer does not vary and becomes independent of the intensity of mixing.

Nebrensky investigates experimentally the heat transfer from a wall at a constant temperature to a mechanically mixed bed of granular material [8, 9]. The effect of rotational speed of a simple paddle mixer, geometrical arrangement of the bed and physical properties of the granular material are determined. From the experimental results obtained, exponents and coefficients are determined in a dimensionless equation found by dimensional analysis:

$$\mathrm{Nu} = 1{,}4.10^{6} \cdot \mathrm{Pe} \cdot \mathrm{Fr}^{-0{,}35} \cdot \left(\frac{\mathrm{P}}{\mathrm{D}}\right)^{-1{,}4} \cdot \left(\frac{\mathrm{L}}{\mathrm{D}}\right)^{-1{,}1} \cdot \left[\frac{(2\mathrm{R} - \mathrm{D})}{2\mathrm{D}}\right]^{-0{,}21} \cdot \theta^{-1{,}3}$$

θ = angle of external friction between the surface of particles and polish steel (rad)

Nu = Nusselt number (appendix 3)
Pe = Peclet number (appendix 3)
Fr = Froude number = $\frac{nD^2}{g}$

g = acceleration of gravity (m/s^2)
n = rotational speed of the mixer (rps)
P = depth of submersion of the mixer (m)
D = diameter of the mixer (m)
L = height of the bed (m)

The research in this topic really moves forward thanks to Schluender whose theory is presented in the next section.

3.2 The particle heat transfer model

3.2.1 Introduction

The works of Schluender and the Institüt für Thermische Verfahrenstechnik der Universität Karlsuhe in the topic of heat transfer between packed, agitated, moving and fluidized beds and

immersed surfaces or walls are remarkable. They could be described by a uniform theory, which considers three basic mechanisms such as: “wall-to-particle” heat transfer, heat conduction in the packed bed (the bed is treated as a quasi-homogenous system) and heat convection by particle motion (for agitated, moving and fluidized beds only).

Both the two first phenomena are well understood and are explained later (3.2.3 and 3.2.4) but the analysis of the phenomenon of heat convection by particle motion is more difficult, mainly due to the fact that this particle motion is not well known in stirred and fluidized beds. Schluender proposes a model which does not need a true description of the particle motion and based on empirical knowledge [10, 11, 12].

3.2.2 Interdependency between the heat transfer and particle motion

Heat transfer between a wall and a bed of particles occurs in a sequence of two steps. In the first step, heat is transferred from a cooling or heating surface (submerged surface or wall) onto the surface of the adjacent layer of particles. Experimentally, a sharp temperature drop at the interface confirms it [12]. The respective heat transfer coefficient is the so-called “wall-to-particle” heat transfer coefficient (α_{wp}). In the second step, heat is transferred into the bed by internal conduction. Internal conduction involves two phenomena: heat conduction and heat convection by particle motion in the case of a fluidized,moving or stirred bed.

As long as the bed is isothermal (there is no temperature gradient within the bed), the second step does not play any role and the “wall-to-bed” heat transfer coefficient is then only related to α_{wp}. Most practical cases involve non-isothermal bed. Consequently, heat conduction within the bed becomes important. However, this mechanism is strongly affected by particle motion.

3.2.3 “Wall surface-to-bed surface” heat transfer (α_{ws})

The fundamental phenomenon involved is the heat conduction through the gaseous gap which separates the particles from the surface. The model is constructed assuming a pointwise contact between the particles and the wall. Taking into account the discontinuity effect at the interfaces, Schluender writes for a single particle the “local wall-to-particle” heat transfer coefficient ($\alpha_{wp,local}$ in $W.m^{-2}.K^{-1}$) due to heat conduction:

$$\alpha_{wp,local} = \frac{k_{gas}}{S+\sigma+\delta} \qquad (3)$$

k_{gas}: heat conductivity of the interstitial gas ($W.m^{-1}.K^{-1}$)
S: local gap width between the surfaces of wall and sphere (m)
δ: sum of wall and particle roughnesses (m)
σ: free path of the gas molecule (m)

$$\sigma = \sigma_o \cdot 2 \cdot \frac{(2-\gamma)}{\gamma} \qquad (4)$$

σ_0: mean free path of the gas molecule (m) which may be calculated according the kinetic theory of the gases (appendix 6, section 3)

γ: accommodation coefficient which may be estimated as given by Martin and reported by Schluender [10] (appendix 6, section 3)

Integration of (3) regardless of the particle radius gives the average value α_{wp} with respect to the projected area of the sphere:

$$\alpha_{wp} = \frac{4k_{gas}}{\overline{d}_S} \cdot \left[\left(1 + \frac{2\sigma + 2\delta \cdot}{\overline{d}_S} \right) \cdot \ln\left(1 + \frac{\overline{d}_S}{2\sigma + 2\delta} \right) - 1 \right] \qquad (5)$$

where $\overline{d}_S$ is the mean particle diameter (m)

The average heat transfer coefficient with respect to the total area of the submerged area of the wall follows from:

$$\alpha_{ws} = \varphi \cdot \alpha_{wp} + (1 - \varphi) \frac{2k_{gas}}{\sqrt{2}/2 \cdot \overline{d}_S + \sigma + \delta} + \alpha_{rad} + \alpha_{dir} \qquad (6)$$

φ: the surface coverage factor = $(1 - \psi)^{2/3}$ (ψ is the void fraction of the bed)

α_{dir} accounts for direct solid to solid heat conduction and may be neglected at normal pressure and for non-metallic particles [12]

α_{rad} accounts for heat transfer by radiation

$$\alpha_{rad} = 4 \frac{C_s}{1/\varepsilon_{wall} + 1/\varepsilon_{bed} - 1} T_{bed}^3 \qquad (7)$$

ε_{wall}, ε_{bed}: emissivities respectively of the wall surface and the bed surface

$C_s = 5.67 \cdot 10^{-8}\ W \cdot m^{-2} \cdot K^{-4}$: Stephan-Boltzman constant

The “wall surface-to-bed surface” heat transfer coefficient (α_{ws}) is a strong function of the physical properties and operating range properties of the gas. The mean diameter of the particles is also an important parameter. It is important to choose a gas with a good conductivity to decrease the contact resistance.

The difficulty to apply this correlation is the estimation of the roughnesses of both surfaces (particle and wall). The wall could be considered as a smooth surface. 10 μm is a common value for most particles according to Malhotra and *al.* [19]. Nevertheless, the particles (rice, steel ball …) used in their experiments have an order of magnitude of the millimetre whereas the particle used in the process have a mean diameter of approximately 200 μm. For Schluender, it can be used to be zero in most practical cases assuming a pointwise contact between the particles and the wall despite the fact that in reality the contact is more pronounced. Probably both effects almost compensate each other. In order to be conservative, 1 μm for the roughness of the particle would be quite a good guess [11, 12].

This model is theoretically built assuming a monodispersed bed of spherical particles which means that all the particles have the same diameter. No paper has been found for polydispersed beds of non-spherical particles although this topic has been subject to current research [12]. However, as we use a broken solid (crushed solid), according [28], the shape seems to have no influence. The fact that the bed is polydispersed should not have a strong

influence on the estimation of the "wall surface-to-bed surface" heat transfer coefficient. Moreover, this coefficient has a limited influence on the "wall-to-bed" heat transfer coefficient (appendix 7).

3.2.4 Heat conduction within a stagnant bed

If the bed is not isothermal, the packed bed may be considered as a quasi-homogenous medium to which Fourier's theory of heat conduction applies.

For a semi-infinite packed bed contacting a plane surface, the Fourier theory yields for the instantaneous "internal heat transfer" coefficient (α_{so} in $W.m^{-2}.K^{-1}$) to the expression:

$$\alpha_{so} = \frac{\sqrt{k_{bed} \cdot \rho_{bed} \cdot C_{bed}}}{\sqrt{\pi \cdot t}} \qquad (8)$$

t: residence time of the stagnant bed (s)
ρ_{bed}: apparent density of the packed bed ($kg.m^{-3}$)
C_{bed}: apparent heat capacity of the packed bed ($J.kg^{-1}.K^{-1}$)
k_{bed}: apparent heat conductivity of the packed bed ($W.m^{-1}.K^{-1}$)

ρ_{bed} is often given by the supplier of the powder, otherwise, it could be measured without difficulties. C_{bed} can be measured in the operating conditions but normally, it is not so far from the value of a single particle. k_{bed} is an important parameter and is the object of the next chapter. The values of the powder characteristics in the SimSan process are presented in the table 1 of the appendix 2. This equation holds for constant surface temperature and not too long residence times which allow having a still non-developed temperature profile within the packed bed.

Integration with respect to time for the time averaged coefficient gives (α_{sb} in $W.m^{-2}.K^{-1}$):

$$\alpha_{sb} = \frac{2}{\sqrt{\pi \cdot t}} \cdot \sqrt{k_{bed} \cdot \rho_{bed} \cdot C_{bed}} \qquad (9)$$

For fully developed temperature profiles at long residence times, Schluender obtains:

$$\alpha_{sb} = \frac{\pi^2}{2} \cdot \frac{k_{bed}}{H} \qquad (10)$$

where H is the height of the packed bed when resting on a horizontal plane surface. In the case of a cylinder, H should be replaced by the radius of the cylinder.

3.2.5 Synthesis for a packed (stagnant) and a perfectly mixed bed

Three cases could be distinguished for a bed:

- More or less mixed (non-perfectly mixed)
- Non-mixed (stagnant bed or packed bed)
- Perfectly mixed

The two last cases are the limiting cases.

The heat transfer coefficient between a plane surface and a stagnant bed drops from α_{ws} at the beginning to $\alpha_{sb}=\pi^2/2.k_{bed}/H$ as the residence time t increases. Below a so-called "critical

time" (t_{crit}), the bed is isothermal because the time required to achieve heat transfer by conduction and to create a temperature gradient within the bed is lower than the residence time. Consequently, the overall heat transfer coefficient (α) is equal to α_{ws}. If the residence time t is higher than t_{crit}, the heat conduction within the bed is involved and α decreases in function of the residence time until $\pi^2/2.k_{bed}/H$ (figure 1).

A perfectly mixed bed is always isothermal so the heat transfer is controlled by the equations (5) and (6). This is to say that α is always equals to α_{ws}.

The heat transfer for non-perfectly mixed beds is expected to be found between the upper and the lower limit as indicated in the figure 1. Below $t_{crit,}$ the upper and lower limits coincide: the degree of mixing and the velocity of the particle motion have no influence on the heat transfer.

Putting α_{ws}= α_{sb} with the help of equations (6) and (9) yields to the critical residence time in seconds:

$$t_{crit} = \frac{4}{\pi}\frac{k_{bed}\cdot\rho_{bed}\cdot C_{bed}}{\alpha_{ws}^2} \qquad (11)$$

According to Schluender [11], t_{crit} might range from milliseconds up to hours, depending on the external conditions (mainly on the gas pressure).

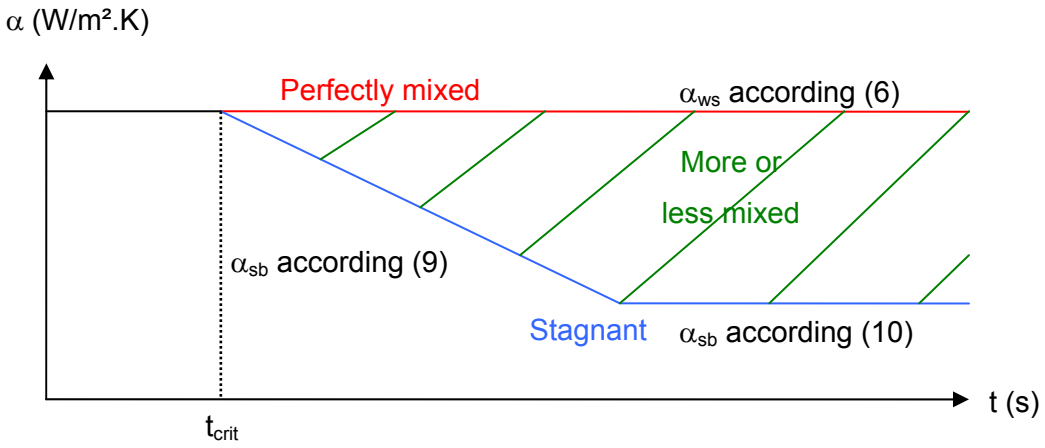

Figure 1: Heat transfer coefficient between a plane surface and an adjacent packed or perfectly mixed bed.

3.2.6 Synthesis for a non perfectly mixed beds: the penetration model

To predict the heat transfer to a non isothermal and non-perfectly mixed bed raises the problem how to predict the particle motion. Since no rigorous theory of the particle motion is available, Schluender has to rely one more or less realistic model. He proposes the "penetration model" used in mass transfer for gas-liquid systems with a good agreement.

He assumes that the condition of non perfect mixing can be described by a periodic sequence of two steps. In the first step, the bed is motionless and the bed is equal to a packed bed. This step is lasting for a certain time t_r at which the bed gains heat through transient heat conduction. The instantaneous heat transfer resistance ($1/\alpha_{mom}$) during this period may be

written approximately as the sum of the wall heat transfer resistance and the internal heat transfer resistance:

$$\frac{1}{\alpha_{mom}} = \frac{1}{\alpha_{ws}} + \frac{\sqrt{\pi \cdot t}}{\sqrt{\rho_{bed} \cdot C_{bed} \cdot k_{bed}}} \qquad (12)$$

where t is the time since the beginning of the period.

The second step occurs after the time t has reached a fictive contact time t_r. Then the packed bed is assumed to become perfectly mixed within a zero time interval. Thereafter, the cycle restarts. This is illustrated in the figure below.

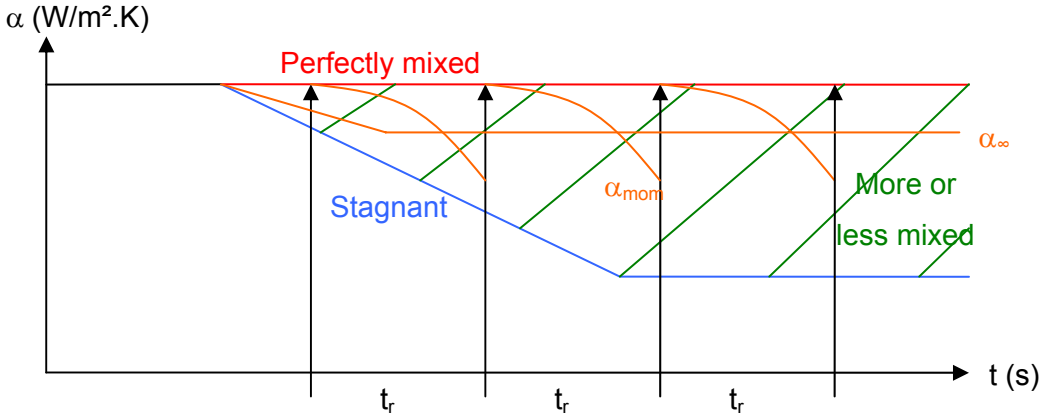

Figure 2: The instantaneous and average heat transfer coefficients according to the penetration model.

Integrating equation (12) with respect to the time gives the steady state heat transfer coefficient α_∞ for a non-perfectly mixed bed, with a constant wall temperature:

$$a_\infty = \frac{2 \cdot \alpha_{ws}}{\sqrt{\pi \cdot \tau}} \left(1 + \frac{1}{\sqrt{\pi \cdot \tau}} \ln \left(\frac{1}{1 + \sqrt{\pi \cdot \tau}} \right) \right) \qquad (13)$$

where τ is the dimensionless fictive contact time according to:

$$\tau = \frac{\alpha_{ws}^2}{\rho_{bed} \cdot C_{bed} \cdot k_{bed}} t_r \qquad (14)$$

The problem with this new equation is that a new variable, the fictive contact time has been introduced. Nevertheless, this variable turns out to be a pure mechanical property of the non-perfectly mixed bed. Consequently, a dimensionless group can be defined (N_{mix}):

$$N_{mix} = \frac{t_r}{t_{mix}} \qquad (15)$$

where t_{mix} is the time constant (s) of the mixing device given by the number of rotations per second of stirrers, scrapers, etc...

Schluender calls N_{mix} the “mixing number” (or “effectiveness of the agitation”). If t_r tends towards 0, it means that the bed is perfectly mixed and then N_{mix} tends towards 0. On the contrary, if t_r tends towards the infinity, it means that the bed is a stagnant one and then N_{mix} tends towards the infinity. If the particles move in plug flow along a rigid wall, N_{mix} equals one

and t_r equals t_{mech}. If they do not, this number must be obtained from experimental data. It is expected to be always greater than one in this case since perfect mixing is not achieved after one revolution of the stirring device.

It may be possible to define another dimensionless group called N_{therm} depending only on the thermal properties of the bed.

$$N_{therm} = \frac{\alpha_{WS}^2 \cdot t_{mix}}{\rho_{bed} \cdot C_{bed} \cdot k_{bed}} \quad (16)$$

And finally, $\tau = N_{mix} \cdot N_{therm}$ (17)

This relation shows the power of the model developed by Schluender. It may be possible to estimate the fictive contact time and consequently the "wall-to-bed" heat transfer coefficient (α) easily with just few parameters. Moreover, this model presents the advantage of being useful for each kind of beds (moving, fluidized and agitated) and for each agitation device (scrappers, blades, screws).

Nevertheless, one parameter must be determined by experiments, the dimensionless group N_{mix} if the bed is not moving as a plug flow. To determine it, a stagnant bed (no particle motion) must be heated with a known heat flux. As α could be evaluated according to Schluender with the residence time of the bed, it may be possible to estimate the heat transfer coefficient linked to the conduction in the wall and the convection of the double mantle ($U_{conv\ \&\ cond}$) by difference with the experimental overall heat transfer coefficient (U). U could be obtained knowing the temperature difference between the coolant and the bed. Then, several experiments in which the bed is heated must be achieved at different stirring velocity. The respective values of α are deduced by difference between U and $U_{conv\ \&\ cond}$. The graph representing α in function of N_{mix} (which depends on the stirring velocity) is drawn. According the relations (13) and (17), N_{mix} can be determined by a curve fitting procedure.

3.3 The "wall-to-bed" heat transfer coefficient with blades

This part deals with the studies of Toei and *al.* focused on granular bed agitated by blades [13, 14]. They show how it is possible to evaluate the heat transfer coefficient with a good agreement between a granular bed and a submerged surface [13] and between a granular bed and a wall [14]. The last reference is summarized below.

The "wall surface-to-bed surface" heat transfer coefficient (α_{ws}) is determined by the model of Schluender (3.2.3). The effect of the heat convection by particle motion can be neglected if the bulk particles are mixed perfectly when the agitator blades scrape them. There is a clearance region between the wall and the blade. Therefore, the heat resistance in this part must be taken into account in addition to the internal heat conduction in the bulk and to the "wall surface-to-bed surface" heat transfer. As it is difficult to estimate this resistance, they introduce the hypothesis that there exists a stationary particle layer which has some effective

thickness δ_e (fig 3). According to this assumption, the heat transfer resistance in the clearance region is equal to δ_e/k_{bed}. The contact time in this case is equal to the interval of the scraping by the agitator blade.

Finally, the time averaged overall heat transfer coefficient is (α in $W.m^{-2}.K^{-1}$):

$$\alpha = \frac{2\alpha_{ws} \cdot k_{bed}}{k_{bed} + \delta_e \alpha_{ws}} \frac{\left(\sqrt{\pi\tau^\circ} - \ln(1+\sqrt{\pi\tau^\circ})\right)}{\pi\tau^\circ} \qquad (18)$$

$$\text{and } \tau^\circ = \frac{\alpha_{ws}^2 \cdot k_{bed} \cdot \pi \cdot (D - 2\delta)}{U \cdot (k_{bed} + \delta_e \alpha_{ws})^2 \cdot C_{bed} \cdot \rho_{bed}} \text{ in seconds} \qquad (19)$$

U: circumferential velocity of the mixer ($m.s^{-1}$)
δ: thickness of the true clearance region (m)
D: diameter of the mixer (m)
α_{ws}, C_{bed}, r_{bed} and k_{bed} have been defined in the previous section

The only unknown parameter is δ_e. According to their experiments, the authors proposed an empirical correlation to estimate it considering the velocity of the agitation, the particle diameter and the clearance region width [14].

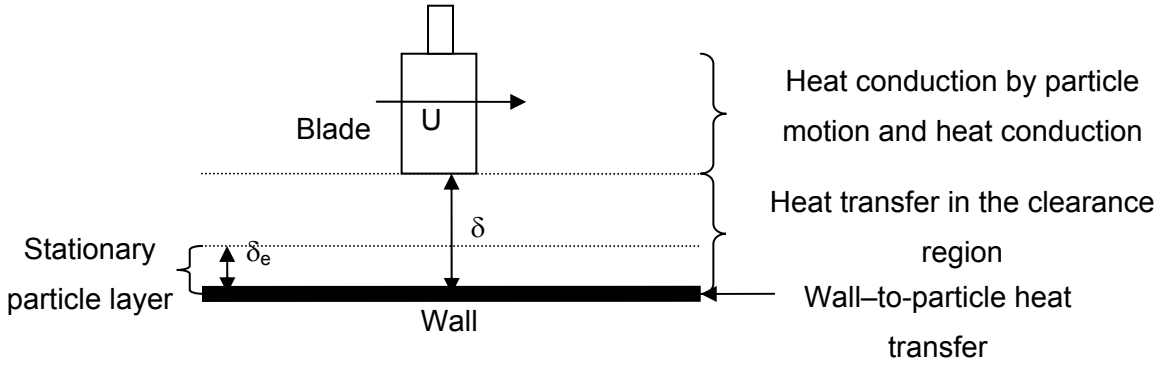

Figure 3: Heat transfer mechanisms

3.4 The model of K. Malhotra and A. Mujumdar

These two authors worked in the field of powders. They tried to characterize the particle flow mechanisms within a granular bed stirred by paddle-types blades [15 to 17] and use this information to construct physically realistic contact heat transfer models with no or minimal adjustable parameters [18 to 20]. As we use a vertical bed, we can not adapt their results concerning the particle motion determined in an horizontal bed. Indeed, a dead volume is present in a horizontal bed. Moreover the gravity is involved in the particle motion so it has an antagonist role in both of these cases (figure 4).

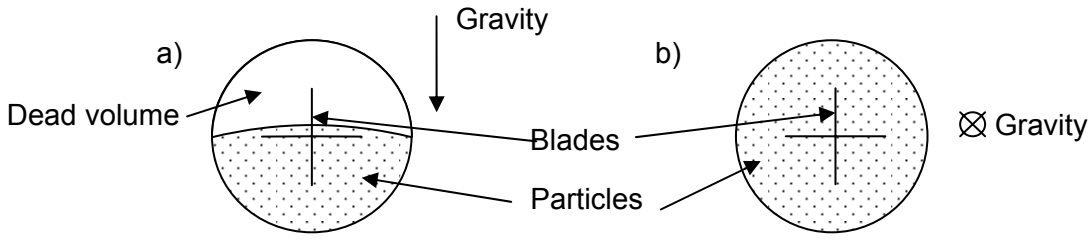

Figure 4: Transversal cut of horizontal (case a) and vertical (case b) beds.

Nevertheless, they developed an interesting heat transfer model in granular beds based on particles renewal rates at the heated or cooled surface. The heat convection by particle motion is neglected as it is explained in [18]. Although this assumption is possible in their operating conditions, it should be used with care in other conditions. Using the packet renewal model, the local "wall-to-bed" contact heat transfer coefficient (h) could be evaluated with the same relation than (13), replacing α_∞ by h. The main difference is that, in the relation (13), we consider a time average coefficient with a fictive contact time unlike the relation given by Malhotra and Mujumdar in which we consider a local coefficient with a true contact time. Consequently, the time average overall heat transfer coefficient (h_{av}) is given by integration with respect to time of h [18].

In the case of particles moving intermittently, the authors proposed a formula to estimate the average contact time. It requires the local efficiency of particle renewal and the number of passes of blade allowing a particle along the wall to traverse the circumferential length of the wall in contact with the particles. These two values must be estimated from experimental observations with a transparent vessel. The calculation depends also of the number of blades.

For the limit case of a plug flow, this model and Schluender's model are equivalent. The true contact time and the fictive contact time are equal like h and h_{av}.

3.5 Conclusion

The models developed in sections 3.3 and 3.4 imply the introduction of more or less arbitrary hypotheses and deal with beds stirred by paddle-type blades. It's the reason why they can not be applied in this study. Nevertheless, by estimating the effectiveness of the agitation (N_{mix}) for a specified granular bed by experiments, it may be possible to calculate the heat transfer coefficient within the bed with a satisfying accuracy [12]. It has been clearly shown that this number is only dependant on the mechanical properties of the stirring device with a given granular material and that neither the temperature nor the pressure influence it.

The heat transfer increases when the particle surface contact time decreases. Indeed, a low value of the particle surface contact time allows replacing more quickly the particles within the bulk material. Two ways are possible to decrease the particle surface contact time: increasing the stirring velocity or reducing as much as possible the thickness of the clearance region between the wall and the edge of the mixer (which allows to facilitate the particles renewal rate in the vicinity of the wall).

Another possibility to support the heat exchange is to choose a carrier gas with a good thermal conductivity since the transfer between the wall and the bed occurs via the gaseous gap between the first layer of particles and the wall.

Moreover, the better the effective conductivity of the bed is and the better the heat transfer is. The next chapter deals with the determination of this parameter for a packed bed with a gas flow.

4 The effective radial conductivity of a packed bed with gas flow

4.1 Introduction

As it is summed up by Smith [29], in a bed of solid particles through which a fluid is passing, heat can be transferred in the radial direction by different mechanisms. Nevertheless, it has been customary to consider that the bed of particles and the gas filled in may be replaced by a hypothetical solid in which conduction is the only mechanism for heat transfer. With such model, the classical Fourier's theory of conduction could be applied. The thermal conductivity of this solid has been called the effective thermal conductivity. This parameter is not an ordinary thermal conductivity, but a property of the bed that depends upon a large number of variables such as gas flow rate, particle diameter, porosity, true thermal properties of the gas and of the solid phases and temperature level.

It may be possible to determine this value experimentally by measuring the radial temperature profile. Nevertheless, some authors tried to find a suitable model in order to estimate with a good agreement the effective thermal conductivity. This is the object of this chapter. Although various papers are available concerning this topic, only the model proposed by Bauer and Schluender is presented. The advantage of this theory is that it is the only one which takes into account the distribution size of the granular material and which proposes some empirical parameters for broken solids (crushed solids like the soda ash). Moreover, this theory needs very simple parameters contrary to the others. Other publications related to this topic include the works of Dixon [24] and Kunii and *al.* [22, 23] who used a quite similar model than Bauer and *al.*.

4.2 The model of Bauer and Schluender

The basis of the method is the assumption that thermal conductivity is the sum of a convective fraction due to the gas flow and of a packing fraction through which the gas does not flow [21]. Radiation and conduction are involved in the packing fraction. The shape of the particles and the size distribution are taken into account. The theory also includes the effect of temperature and pressure as well as the thermal characteristics of the solid and fluid phases.

Thus, in a dimensionless form:

$$\frac{k_{bed}}{k_{gas}} = \left(\frac{k_{bed}}{k_{gas}}\right)_{convection} + \left(\frac{k_{bed}}{k_{gas}}\right)_{\substack{conduction \\ radiation}} \qquad (20)$$

k_{bed} is the effective thermal conductivity of the bed and k_{gas} the thermal conductivity of the gas. These terms are related to the different fractions of heat transfer.

According to [21], part I: $$\left(\frac{k_{bed}}{k_{gas}}\right)_{convection} = \frac{Pe_x}{K} = \frac{m_o Cp_{gas}}{k_{gas}} \cdot \frac{x_F}{K} \qquad (21)$$

Pe_x is a Peclet number formed with a mixing length x_F where convection transfer occurs. m_o is the surface mass flow rate of the gas ($kg.m^{-2}.s^{-1}$) and Cp_{gas} is the heat capacity ($J.kg^{-1}.K^{-1}$) of the gas at the bed temperature. K is a constant which depends on the ratio between the bed diameter and the mean particles size.

According to [21], Part II

$$\left(\frac{k_{bed}}{k_{gas}}\right)_{\substack{\text{conduction}\\ \text{radiation}}} = \left(1-\sqrt{1-\psi}\right)\cdot\left[\frac{\psi}{(\psi-1)+\frac{k_{gas}}{k_D}}+\psi\frac{k_R}{k_{gas}}\right]+\sqrt{1-\psi}\cdot\left[\varphi\frac{k_S}{k_{gas}}+(1-\varphi)\frac{k^*_{bed}}{k_{gas}}\right] \quad (22)$$

This ratio depends of the porosity (void fraction) of the bed (ψ). φ accounts for the fraction of the heat transfer due to possible contact surfaces between particles. k_S is the mean thermal conductivity of the solid phase and k_R and k_D are equivalent thermal conductivities between the surfaces of the solid phase due to thermal radiation and Smoluchowski effect. This effect is an additional heat-transfer resistance which appears by considering that in a vapour space bounded by solid bodies, the normal movement of the gas molecules is inhibited at the boundary surfaces. k^*_{bed} corresponds to the transfer through two particle halves that are separated by a wedge of gas. The details of the formulation of each component are described in appendix 6.

The effective thermal conductivity is a parameter which takes into account the three possible means (radiation, convection, conduction) of transfer in just one concept. This is the advantage of considering the bed as a homogenous system. The other theories developed for the effective thermal conductivity need more complicated parameters and don't take into consideration the size distribution of the granular materials. Some of them don't consider the gas in the void fraction. The thermal conductivity of the interstitial gas contributes to the effective thermal conductivity in a significant way by two means. Indeed, the heat is not only exchanged through the particles in the bed but also through the void fraction. Moreover, in the case of a turbulent flow, heat could be exchanged by convective mixing.

4.3 Conclusion

It may be possible to estimate with a quite good accuracy the effective radial thermal conductivity of a packed bed using the model of Bauer and Schluender.

We should take into account the influence of the reaction as mentioned by Smith [19]. Indeed, reactions generate a difference between the gas and the surface of the particles temperatures. Nevertheless, homogenous models with particles and gas which have the same temperatures are currently used such as the model of Bauer and Schluender. Few publications have been found concerning this topic. Thus, as mentioned Wijngaarden and Westerterp [25], if an exothermic reaction is carried out, the particle temperature will be higher than the gas

temperature. Consequently, as the reaction rate is a function of the temperature of the particle's surface, this one will be higher than expected leading to a more pronounced temperature profile. It is the contrary with an endothermic reaction. However the authors are convinced that the system properties remain constant and are not influenced by a chemical reaction. They feel there is no reason to assume that k_{bed} is changed when a chemical reaction occurs.

There is another parameter to take into account. At the beginning of the conversion, the particles involved are not really particle of soda ash because of the coating. The true diameter must be higher than the experimentally found one. Moreover during the conversion, the coating disappeared and the stirring device causes attrition. Nevertheless, simulations show that increasing or decreasing the mean diameter by 30 % induces a variation of k_{bed} of 3%.

Furthermore, the conductivity of the sodium carbonate particles is used for the contact heat transfer between the particles. However, the contact which really occurs involves sodium layers at the beginning of the conversion. We can show that this has no influence, according to equation (6) in appendix 6 and by taking into consideration the conductivity of the sodium.

5 Study of the heat transfer in the pilot

5.1 Introduction

During the first experiments carried out with the paddle-type stirring device (operating conditions in section 1.3), the overall heat transfer has been determined during the oxidation step. Different amounts of sodium have been introduced (2 and 5 kg). The inlet temperature of the oil is monitored until steady state is reached at given O_2 and CO_2 flow rate. The temperatures of the bed and the oil are measured and the difference is reported. The temperature of the oil is constant between the inlet and the outlet of the double mantle taking into account the heat loss through the insulation (appendix 4) of approximately 300 W. Indeed, a heat flux of 3000 W induces only an increase of this temperature of more or less 1K ($\Delta\theta =$ heat flux/(Oil flow * Oil heat capacity)). CO_2 and O_2 are the limiting reagents and are totally consumed. The results are presented below.

Na batch (kg)	O_2 flow rate (NL/min)	CO_2 flow rate (NL/min)	Theoretical heat flux (W)		Measured Temp. difference ($\Delta\theta$)	Heat transfer coef. (W/m².K)	
			100% Na_2O	100% Na_2O_2		100% Na_2O	100% Na_2O_2
2	2	1	1494	1126	15,7	158	119
5	3	2	2358	1868	25	158	124
5	4	3	3223	2610	34	157	127

Table 3: Heat exchange coefficients in the pilot during the oxidation step

Since the ratio between the both possible reaction pathes is not precisely known, the theoretical fluxes can not be exactly calculated. Nevertheless, the maximal and minimal values can be determined assuming respectively a complete conversion in sodium oxide and sodium peroxide. For each case, the theoretical flux is calculated using the gas flow rates and the enthalpies of reaction at 300°C which is approximately the measured temperature of the bed. The overall heat transfer coefficients linked to each case are calculated according to the Newton's law (appendix 3) taking the inner effective surface of contact between the bed and the wall (A_{bed}) as the surface of reference. It appears that the overall heat transfer coefficient varies between 120 and 160 $W.m^{-2}.K^{-1}$ depending on the hypothesis.

The aim of the next sections is to estimate by a theoretical approach the overall heat transfer coefficient in the SimSan pilot, to compare the value found with argon as interstitial gas with the experimental results and to emphasize the influence of the carrier gas choice.

5.2 Expression of the overall heat transfer coefficient

According to 2.5, we consider that the heat transfer (Q) occurs from the bed to the inner wall, through the wall by conduction and finally from the wall to the coolant by forced convection.

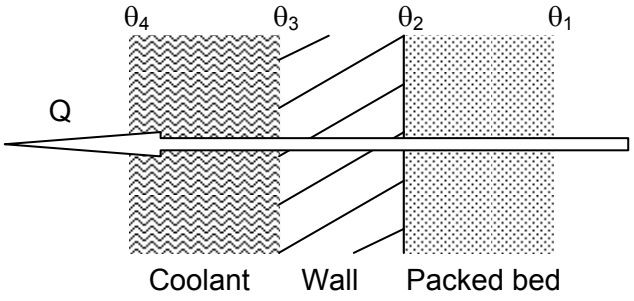

Between the bed and the wall:

$$Q = \alpha \cdot A_{bed} \cdot (\theta_1 - \theta_2) \qquad (23)$$

In the wall:

$$Q = K \cdot (\theta_2 - \theta_3) \qquad (24)$$

Between the wall and the coolant

$$Q = h_{oil} \cdot A_{oil} \cdot (\theta_3 - \theta_4) \qquad (25)$$

A_{bed}: Effective surface of contact between the bed and the wall (m^2)
A_{oil}: Effective surface of contact between the oil and the wall (m^2)
α: "wall-to-bed" heat transfer coefficient ($W.m^{-2}.k^{-1}$)
h_{oil}: convection coefficient of the coolant ($W.m^{-2}.k^{-1}$)

The heat transferred by conduction in the wall is the sum of two contributions: the heat exchanged by the cylindrical wall and the heat exchanged by the bottom of the vessel (see the technical drawings). According to the section related to the conduction in appendix 3:

$$K = k_{wall} \cdot \left(\frac{2 \cdot \pi \cdot L_{mantle}}{\ln\left(d_{ext} / d_{int} \right)} + \frac{A_{bot}}{t_w} \right) \qquad (26)$$

k_{wall} : conductivity of the wall ($W.m^{-1}.k^{-1}$)
L_{mantle}: height of the bed (m)
d_{ext}: external diameter of the wall (m)
d_{int}: internal diameter of the wall (m)
A_{bot}: surface of the bottom of the vessel in contact with the double mantle (m^2)
t_w: thickness of the wall (m)

All the data linked to these parameters are presented in appendix 2.

Isolating the three differences of temperature for relations (23) to (25) and doing the sum of each one lead finally to:

$$\theta_1 - \theta_4 = Q \cdot \left(\frac{1}{A_{oil} \cdot h_{oil}} + \frac{1}{\alpha \cdot A_{bed}} + \frac{1}{k_{wall}\left(2 \cdot \pi \cdot L_{mantle} \Big/ \ln\left(d_{ext} \Big/ d_{int} \right) + \frac{A_{bot}}{t_w} \right)} \right) = \frac{Q}{U \cdot A} \qquad (27)$$

Thus, it is possible to express the heat flux Q in function of the difference of temperature between the bed and the coolant. The only unknown parameters to determine are h_{oil} and α.

5.3 Determination of the "wall-to-bed" heat transfer coefficient in function of the gas used

The coefficient α could be determined using the model of Schluender. Nevertheless, three parameters are needed, the "wall surface-to-bed surface" heat transfer coefficient (α_{ws}), the effective thermal conductivity ($k_{e\ or}\ k_{bed}$) and the mixing number(N_{mix}).

5.3.1 The "wall-to-bed surface" heat transfer coefficient in the pilot

The temperature and the pressure have been fixed at respectively 200°C and 1,013 bar. The real temperature of the gas in the vicinity of the wall is not well known.Therefore the minimal physically possible value in the pilot leading to the lower coefficients has been chosen in order to be conservative. The dimensionless emissivity of the particles are unknown. Nevertheless, taking it as 1 leads to a maximum contribution of the radiation (α_{rad}) of 8 W (assuming that the particle temperature is not significantly higher than the average bed temperature), which can be neglected according to the final results presented below. Estimating the roughness of the wall and of the particles is more problematic. The wall can be considered as a smooth surface. Nevertheless it does not seem to be the case of the particles. In order to be conservative, the value of 1 μm has been chosen (3.2.3).

	Ar	**N_2**	**He**
σ_o (m)	1,26E-07	1,07E-07	2,18E-07
γ	0,73	0,76	0,22
σ (m)	4,4E-07	3,5E-07	3,5E-06
α_{WP} ($W.m^{-2}.K^{-1}$)	1637	2463	9288
α_{WS} ($W.m^{-2}.K^{-1}$)	**1044**	**1566**	**6278**

Table 4: "Wall to bed surface" heat transfer coefficient in function of the interstitial gas

The coefficient found is slightly underestimated. Nevertheless, an exact value is not really needed (appendix 7). It appears that Helium provides a coefficient 3 or 4 times better than the other possible carrier gases. This is mainly due to the thermal conductivity of this gas which is more or less 5 times higher. Moreover, the accommodation coefficient is lower, which induces

a free path (σ) ten times higher.

5.3.2 The effective thermal conductivity

The effective thermal conductivity has been calculated considering gas flow rates slightly lower than the minimum of fluidization (appendix 2, table 7). It appears that with such low flow rates, the convective fraction could be neglected. The temperature of the gas has been chosen equals to 200 °C in the range 200-300 °C considering the worst case (lowest effective thermal conductivity). According to [26], the true thermal conductivity of the sodium carbonate particles is equal to 0,53 $W.m^{-2}.K^{-1}$. The main results are presented below in the table 5. The radiative contribution ($(k/k_{gas})_{convective}$) and the radiative fraction (k_R/k) are negligible. Due to the good thermal conductivity of the Helium, the effective thermal conductivity with a flow of Helium can be two times higher than with Argon.

	Ar	N2	He
Flow rate of gas ($NL.min^{-1}$)	8	10	90
Pe	0,01316	0,01585	0,01819
(k/k_{gas}) convective	0,0016	0,0020	0,0023
(k_R/k)	4E-09	2E-09	4E-10
(k/k_D)	1,00	1,00	1,01
(k_s/k)	20,3	13,8	2,5
K	0,86	0,79	-0,14
$(k_{SO}*/k)$	7,1	5,8	2,0
(k/k_{gas}) conductive	4,85	4,07	1,60
(k_{bed}/k_{gas})	4,85	4,07	1,60
k_{bed} ($W.m^{-1}.K^{-1}$)	**0,13**	**0,16**	**0,34**

Table 5: Effective thermal conductivity in the pilot in function of the carrier gas

5.3.3 The “wall-to-bed” heat transfer coefficient

According to the section 3.2.6, it may be possible to estimate the heat transfer coefficient (α) between the bed and the wall. The only parameter unknown at this time is the dimensionless number N_{mix}.

The first device of agitation in the pilot was made of blades with scrappers. With a quite similar device (blades and brushes), Schluender found a mixing number of approximately 3 [12] but the two components were used at the same velocity. However, in the pilot, the scrappers and the blades do not turn at the same velocity and the model of Schluender can not be used. Nevertheless, to obtain an order of magnitude of α, we can consider in first approximation that the scrappers allow to have a plug flow of particles near the wall at a very low velocity (15 rpm) in the vicinity of the wall. Consequently, N_{mix} is taken equal to one. The contribution of the blades which turn at a high velocity is neglected and the value of α may be underestimated.

	Ar	N_2	He
N_{therm}	26.55	48.17	357.41
τ	26.55	48.17	357.41
α ($W.m^{-2}.K^{-1}$)	**171**	**201**	**335**

Table 6: Underestimated "wall-to-bed" heat transfer coefficient using Ar, N_2 and He with the paddle-type device

In the case of the new device with a helicoïdal screw (165 rpm), a plug flow of particles is expected leading to a mixing number equals to one (table 7):

	Ar	N_2	He
N_{therm}	2.41	4.38	32.46
τ	2.41	4.38	32.46
α ($W.m^{-2}.K^{-1}$)	**394**	**492**	**947**

Table 7: Expected "wall-to-bed" heat transfer coefficient with a helicoïdal screw

The heat exchange coefficients in the bed seem to increase more than two times using a helicoïdal screw. Nevertheless, with this design, the result is achieved with an energy consumption and an attrition of the particles really lower due to the low velocity of the agitation. In the future, it would be necessary to determine the mixing number experimentally to improve this estimation (procedure in the section 3.2.6).

5.4 Determination of the convection coefficient of the coolant

In the double mantle, the coolant flows at 70L/min at a temperature of approximately 280°C to cool down the bed of particles. A such high temperature has been chosen during the experiments in order to avoid that the temperature of the inner wall in contact with the particles goes down below 270°C which is the minimal temperature to achieve the conversion.

The convection coefficient in the bottom of the double mantle is assumed to be equal to the one of the cylindrical part. The bypass section of the fluid is equal to 0,066 m^2 (A_{bypass}) and the equivalent diameter to 0,210 m (D_{eq}). Considering the thermal properties of the Marlotherm (appendix 2, table7) leads to:

Pr = 11,3

Re = 7269

As Re > 2300, the correlation (8) presented in appendix 3 has been used leading to a Nusselt number of 106.

Finally the convection coefficient in the double mantle (h_{oil}) is equal to 53 $W.m^{-2}.K^{-1}$.

The calculated coefficient is particularly low. Indeed, the thermal properties of the Marlotherm are not really good at this temperature (low thermal conductivity) and the turbulent regime is not clearly established due to a bypass section too important. Other correlations have been tested and seem to confirm the order of magnitude of this coefficient (Dietus-Boltern and Hausen correlations).

5.5 Determination of the heat transfer resistance in the pilot

According to the equation (27), the heat transfer resistance in the pilot between the bed and the coolant (1/U.A (in K/W)) could be evaluated assuming α equals to 170 $W.m^{-2}.K^{-1}$ and h_{oil} to 53 $W.m^{-2}.K^{-1}$. The values of the other parameters needed are presented in appendix 2.

U.A was found to be approximately equal to 30 $W.K^{-1}$. Consequently, taking A_{bed} as the surface of reference leads to an overall heat transfer coefficient of 50 $W.m^{-2}.K^{-1}$ whereas a value of approximately 140 $W.m^{-2}.K^{-1}$ was found experimentally. This difference may be due to an underestimation of the convection coefficient in the double mantle. Such value found theoretically is clearly dominant and the other resistances (in the bed and in the wall) have a limited influence on the global heat transfer coefficient.

The presence of turbulence promoters (gutter, coil or baffle) in the double mantle which are not drawn in the specifications has been firstly considered to explain this difference. The supplier confirmed that no turbulence promotors are present within the double mantle. The fact that the coolant flow rate is not clearly known and that the correlations used are empirical could be also evoked as possible reasons.

5.6 Conclusion

The heat transfer coefficient found by the calculations is two times lower than the one found experimentally maybe due to an underestimation of the convection coefficient in the double mantle which has been found to be the limiting factor contrary to the intuition. The reason of such disagreement is still unexplained.

Consequently, it has not been possible to check if the “wall-to-bed” heat transfer coefficient estimated by the model of Schluender is in agreement with the experimental value. Nevertheless if the convection is really the limiting factor, it would be possible to reduce considerably the temperature of the coolant in the double mantle leading to a higher temperature gradient and then to a higher heat flux.

Several tests are possible to check if the convection is the limiting factor. It may be possible to study the heating of a compound with known thermal properties. Another way is reducing the velocity of the agitation or changing the carrier gas and reporting their respective influences.

In the future, it would be interesting to check the model of Schluender applied in our case and determine the mixing number. It appears that Helium could be an interesting choice for its excellent thermal properties (high heat capacity and high thermal conductivity). Nevertheless, Helium is significantly more expensive than the two other candidates.

Conclusion

SCK•CEN would like to develop through the SimSan project a suitable process to convert the contaminated metallic sodium in an inert powder of sodium carbonate. The feasibility has been shown but the conversion rate is still limited by the heat transfer rate between the mechanically agitated bed and the coolant which flows in the double mantle.

The heat transfer coefficient between the bed and the wall has been estimated in the pilot according to the model of Schluender where the packed bed is assumed to be an homogenous system in which the Fourier's theory of conduction could be applied. This model is constructed theoretically but requires the determination of an experimental parameter, the mixing number (N_{mix}). Indeed, the particle motion is brought into play in the expression of the heat transfer coefficient.

The contact resistance between the first layer of particles and the wall (α_{WS}) and the effective conductivity of the bed (k_{bed}) are also essential for the determination of the "wall-to-bed" heat transfer coefficient. These parameters must be calculated taking into account the physical properties of the granular material, the thermal properties of the gas and its flow rate.

The agreement of this theory with the experiments has not been verified yet. Nevertheless, it will be possible to verify the model of Schluender and to estimate the mixing number with the experiments which will be carried out in a reactor equipped with a helicoïdal screw.

Simple statements follow from the study of the different models presented in this report. The choice of the inert gas appears to be fundamental as the heat transfer coefficient in the bed depends, by several ways, on the thermal conductivity of the gas and increases with it. Helium seems to be a good choice. Another important parameter is the design of the agitation device. With helicoïdal screws, a plug flow of particle is expected leading to a good efficiency of the mixing and less attrition than the other kinds of devices. Moreover, the distance between the wall and the screw must be as low as possible in order to improve the renewal of the particles at the cooling surface. However, as the minimum of fluidization velocity of the bed is low, the convective effect due to the turbulences of the gas flow is negligible.

In the pilot settled in BR3, the convection in the double mantle seems to be the limiting factor of the heat transfer. If it is really the case, it means that the velocity of the agitation and the nature of the gas have a limited influence on the heat transfer rate. Testing their influence would be a mean to check it. Decreasing the temperature of the coolant would be another interesting evolution. It would allow to increase the gradient of temperature and then improve the heat transfer rate. However, the convection coefficient decreases with the coolant temperature which emphasizes the presence of an optimal temperature which must be determined.

References

Publications

1 J.S.M Botterill and M. Desai, *Powder Technology*, vol. 6, 1972

2 T. Otake, S. Tone, *Technol. Repts. Osaka Univ.,* Vol. 10, 1960

3 T. Otake, S. Tone, *Chem. Eng*.,1961

4 J.S.M. Botterill, Garner F.H., Ross D.K., *Chem. Age India*, Vol.12, 1961

5 J.S.M. Botterill, K.A. Redish, Ross D.K., J.R. Williams, *Symposium on the interaction between fluids and particles, London*, 1962

6 V.D. Dunskij, *Inz. Fiz*, Vol. 7, 1964

7 V.D. Dunskij, *Vsesojuznoe Sovescanie po teplo- i massoobmenu*, *Minsk*, 1964

8 J. Nebrensky, Heat transfer to a mechanically mixed bed of granular material, *Collection of Czechoslovak Chemical Communications*, Vol. 31, 1966

9 J. Nebrensky, Mechanism of heat transfer to a mechanically mixed bed of granular material, *Collection of Czechoslovak Chemical Communications*, Vol. 31, 1966

10 E.U. Schluender, Heat transfer between packed, agitated and fluidized beds and submerged surfaces*, Chem. Eng. Commun.*, vol. 9, 1981

11 E.U. Schluender, Particle heat transfer, *Proceedings of the 7th International Heat Transfer Conference, Munich*, vol. 1, 1982

12 E.U. Schluender, Heat transfer to packed and stirred beds from the surface of immersed bodies, *Chem. Eng. Process*, vol. 18, 1984

13 R. Toei, T. Ohmori and M. Okazaki, heat transfer from submerged body moving in granular bed, *Drying 85*, 1985

14 R. Toei, T. Ohmori, T. Furuta and M. Okazaki, heat transfer coefficient between heating wall and agitated granular bed, *Drying 85*, 1985

15 K. Malhotra, A. Mujumdar, Fundamental particle mixing studies in an agitated bed of granular materials in a cylindrical vessel, *Powder Technology*, 1988, vol. 55

16 K. Malhotra and A. Mujumdar, Particle mixing and solids flowability in granular beds stirred by paddle-type blades, *Powder Technology*, 1990, vol. 61

17 K. Malhotra, A. Mujumdar and M. Miyahara, Estimation of particle renewals rates along the wall in a mechanically stirred granular bed, *Chem. Eng. Process*, 1990, vol. 27

18 K. Malhotra and A. Mujumdar, Model for contact heat transfer in mechanically stirred granular beds, *Int. J. of Heat and Mass Transfer*, 1991, vol. 34

19 K. Malhotra and A. Mujumdar, Wall-to-bed contact heat transfer rates in mechanically stirred granular beds, *Int. J. of Heat and Mass Transfer*, 1991, vol. 34

20 K. Malhotra and A. Mujumdar, Particle flow and contact heat transfer characteristics of stirred granular beds, *Drying technology*, 1992, vol. 10

21 R. Bauer and E.U. Schluender, Effective radial thermal conductivity of packings in gas flow. Part I, Convective transport coefficient, Part II, thermal conductivity of the packing fraction without gas flow, *Int. Chem. Eng*., Vol. 18, 1978

22 S. Yagi and D. Kunii, Studies on effective thermal conductivities in packed beds, *AIChE Journal*, Vol.3, 1957

23 G.P. Willhite, D. Kunii and J.M. Smith, Heat transfer in beds of fine particles (heat transfer perpendicular to flow), *AIChE Journal*, Vol.8, 1961

24 A.G. Dixon, Thermal resistance models of packed-bed effective heat transfer parameters, *AIChE Journal*, 1985, Vol. 31

25 R.J. Wijngaarden and K.R. Westerterp, Do the effective heat conductivity and the heat transfer coefficient at the wall inside a packed bed depend on a chemical reaction? Weaknesses and applicability of current models, *Chem. Eng. Sc.*, Vol.44, 1989

26 A.M. Abousehly, M.M. Ibrahiem, M.T. Desouky, A.M. Abdel-Rahman and M. Tag-Alden, Measurement of the thermal properties of Li_2CO_3, Na_2CO_3, Li_2CO_3, $CaCO_3$, $MgCO_3$, $NiCO_3$ in the temperature range 300-700 K by the heat flash technique, *High Temperatures-High pressures*, 1996

27 K. Malhotra and A. Mujumdar, Effect of particle shape on particle-surface thermal contact resistance, *Journal of chemical engineering of Japan*, Vol. 23,1990

Books

28 M. Jacob, *Heat transfer*, vol. 2, 1957

29 J.M. Smith, *Chemical engineering series*, 1956

30 V. Cavaseno, *Process heat exchange*, 1979

31 R. Gibert, *Génie chimique, tome 2 : Transmission de la chaleur*, 1963

32 A.B. De Vriendt, *La transmission de la chaleur, vol.1,* 1982

Intern documentation

33 E. Cantrel, *SimSan : Technical report*, 2005

34 E. Cantrel, J. braet, J. Seghers, *SimSan Project: feasibility demonstration with 1 kg sodium*, 2004

35 E.Cantrel, P. Cnapelinckx, J. Seghers, *Belgatom/SCK•CEN technical workshop on SimSan project:* 2004

Appendixes

Appendix 1

The technical drawings

Figure 1: Flowsheet of the SimSan pilot installation

Figure 2: The reactor MSR with the paddle type and scrappers stirring device

Figure 3: The reactor MSR with the helicoïdal screw

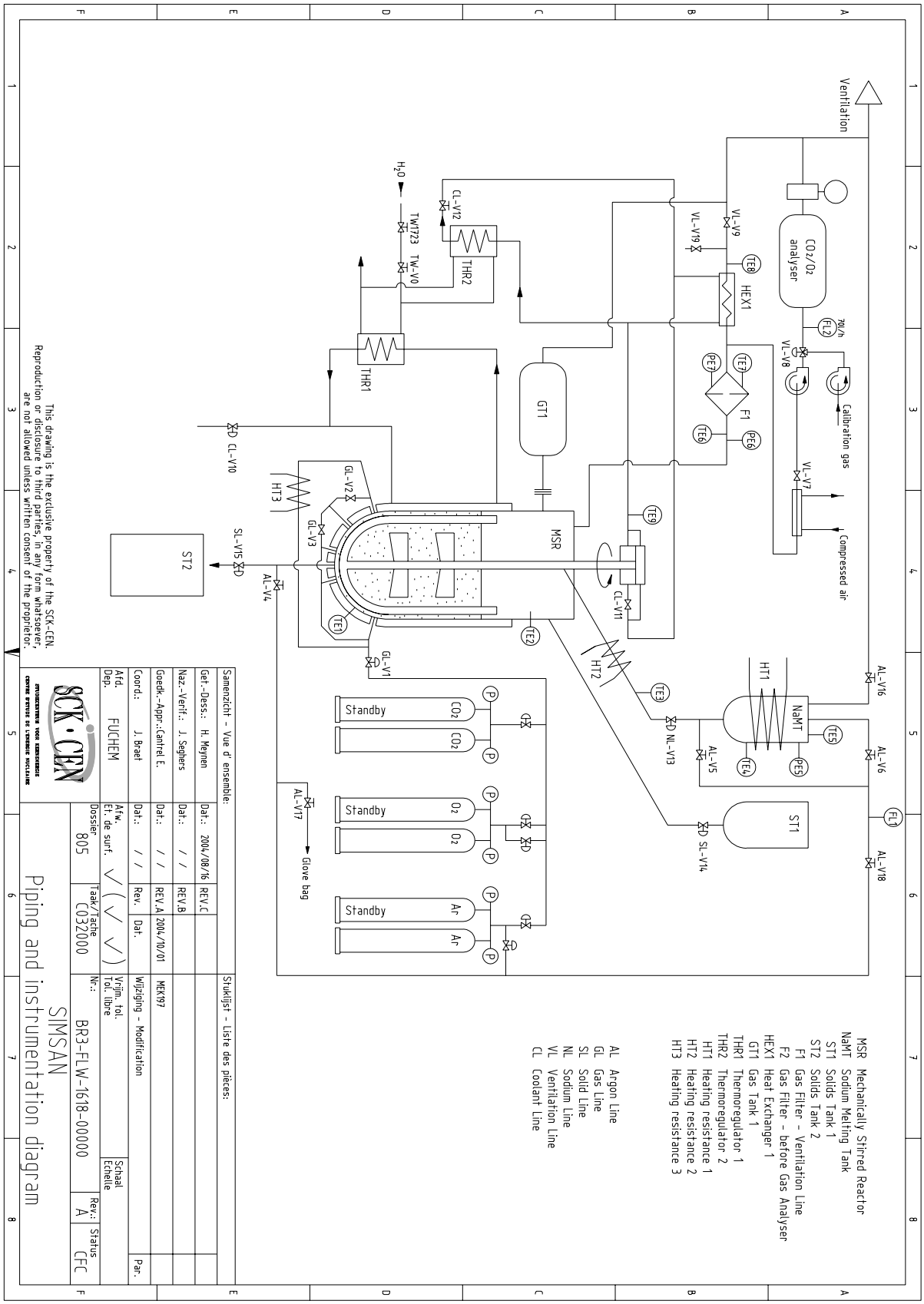

Figure 1 : Flowsheet of the SimSan pilot

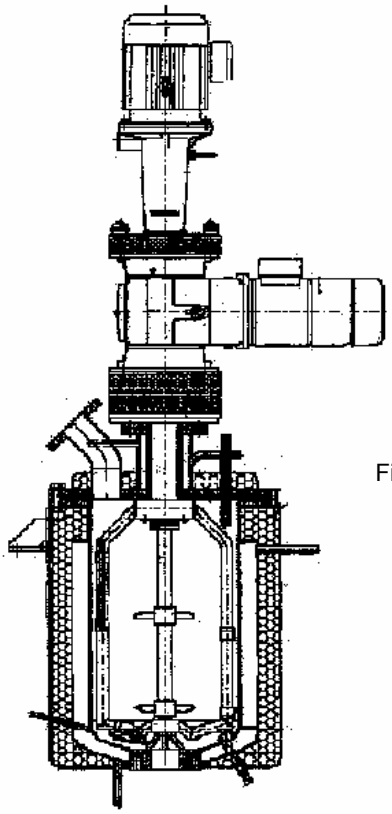

Figure 2: The reactor MSR with the paddle type and scrappers stirring device

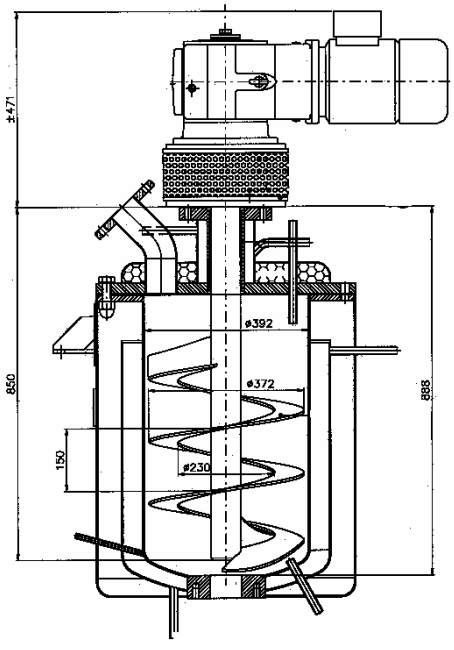

Figure 3: The reactor MSR with the helicoïdal screw

Appendix 2

The operating and technical characteristics

Properties of the sodium carbonate

Main characteristics of the bed

Thermal properties of the materials used in the pilot

Surfaces of heat exchanges in the pilot

Means dimensions of the reactor MSR

Thermal properties of the coolant: Marlotherm® SH

Determination of the minimum of fluidization of the bed in the reactor MSR

Thermal properties of Argon, Nitrogen and Helium between 400 and 700 K at 1 bar

Molecular mass	M_{Na2CO3}	0,10599	$kg.mol^{-1}$
carbonate melting point	T_{melt}	854	°C
particle density	ρ_p	2532	$kg.m^{-3}$
bed density	ρ_b	1000	$kg.m^{-3}$
porosity	ψ	0,6	
mean diameter of the particles	$\bar{d}$	≈200	μm
bed thermal heat capacity	C_{bed}	1300	$J.kg^{-1}.K^{-1}$
particle thermal conductivity	k_S	0,53	$W.m^{-1}.K^{-1}$
particle emissivity	ε	unknown	
particle roughnesses	δ	unknown	m

Table1: Properties of the sodium carbonate

diameter of the bed in the pilot	d_{bed}	0,392	m
mean temperature of the bed	T_{bed}	300	°C
amount of carbonate in the pilot	m_{matrix}	50	kg
bed height in the pilot	H_{bed}	0,41	m
bed volume in the pilot	V_{bed}	50	L
volume of the void fraction	V_{void}	30	L

Table 2: Main characteristics of the bed

wall (Steel 316) thermal conductivity	k_{wall}	18,9	$W.m^{-1}.k^{-1}$
insulation thermal conductivity	$k_{insulation}$	0,064	$W.m^{-1}.k^{-1}$
wall (Steel 316) emissivity	ε_{wall}	0,18	

Table 3: thermal properties of the materials used in the pilot

length of the gas phase	L_{gas}	0,256	m
heat exchange area between the bottom of the vessel and the mantle	A_{bot}	0,094	m^2
heat exchange area between the inner wall and the gas phase	A_{gas}	0,179	m^2
heat exchange area between the inner wall and the bed	A_{bed}	0,614	m^2
heat exchange area between the coolant and the wall of the vessel	A_{oil}	0,798	m^2
total heat exchange area between the coolant and the vessel	A_{tot}	0,783	m^2
heat exchange area between the coolant and the insulation	A_{ins}	1,049	m^2
heat exchange area between ambient air and the insulation cylinder	A_{cyl}	1,422	m^2
heat exchange area between air and the bottom of the insulation	A_{plate}	0,275	m^2

Table 4: Surfaces of heat exchanges in the pilot

internal diameter of the vessel	d_{int}	0,392	m
thickness of the vessel's wall	t_w	0,004	m
external diameter of the vessel	d_{ext}	0,400	m
internal diameter of the double mantle	D	0,494	m
equivalent diameter of the double mantle	D_{eq}	0,210	m
thickness of the double mantle wall	t_{dm}	0,003	m
internal diameter of the insulation	D_{int}	0,500	m
external diameter of the insulation	D_{ext}	0,620	m
thickness of the insulation	$t_{insulation}$	0,060	m
external diameter of the attach unloading		0,185	m
height of the vessel	L_{vessel}	0,670	m
height of the double mantle	L_{mantle}	0,560	m
height of the insulation cylinder	L_{cyl}	0,730	m
width of the bottom of the insulation	$L_{bot}=D_{int}$	0,620	m
bypass section of the fluid in the double mantle	A_{bypass}	0,066	m²

Table 5: Means dimensions of the reactor MSR

Temper.	**Density**	**Specific heat**	**Thermal conductivity**	**Viscosity**		**Vapour**
				Dynamic	**Cinematic**	
°C	**kg.m^{-3}**	**kJ.kg^{-1}.K^{-1}**	**W.(m.K)$^{-1}$**	**cp (10³ Pa.s)**	**cSt (10^{6} m²/s)**	**hPa**
0	1058	1.48	0.133	337	321	
20	1044	1.55	0.131	49	47	
40	1030	1.62	0.128	17	16.5	
60	1016	1.7	0.125	8.2	8.1	
80	1001	1.77	0.123	4.8	4.7	
100	987	1.85	0.12	3.2	3.1	
120	973	1.92	0.117	2.3	2.3	
140	958	1.99	0.115	1.7	1.8	0.1
160	944	2.07	0.112	1.3	1.4	0.5
180	930	2.15	0.11	1.1	1.2	1.7
200	915	2.22	0.107	0.84	0.92	5
220	901	2.29	0.104	0.7	0.77	12
240	887	2.37	0.102	0.58	0.65	27
260	873	2.44	0.099	0.5	0.57	54
280	858	2.52	0.096	0.43	0.5	98
300	844	2.59	0.094	0.38	0.45	200
320	830	2.67	0.091	0.33	0.4	315
340	815	2.74	0.088	0.29	0.35	560
360	801	2.82	0.086	0.26	0.32	860

Table 6: Thermal properties of the coolant: Marlotherm® SH

	Ar	N_2	He
ρ_f (kg.m^{-3})	1,01	0,67	0,67
μ_f (Pa.s)	3,2E-05	2,6E-05	2,8E-05
Ga	23,5	24,2	20,5
Re_{mf}	0,02	0,02	0,01
U_{mf} (m.s^{-1})	3,8E-03	4,7E-03	4,3E-03
F_{mf} (NL.min^{-1})	15	18	118
Re_p (with U_{mf})	0,01	0,01	0,01

Table 7: Determination of the Minimum of fluidization of the bed in function of the gas used in the reactor MSR

As the gas enters at 200°C, the minimum of fluidization has been calculated using the properties of the gas at this temperature. The correlation of Leva has been used in laminar regime (Rep ≤ 10):

$$U_{mf} = 0{,}005 \cdot \frac{\psi_{mf}^3 \cdot \varphi^2}{1-\psi_{mf}} \cdot g \cdot (\rho_p - \rho_f) \cdot \frac{d_p^2}{\mu_f}$$

ρ_p: particle density (kg.m^{-3})
ρ_f: gas density (kg.m^{-3})
μ_f: gas dynamic viscosity (Pa.s)
d_p: particle diameter (m)
φ: sphericity
ψ_{mf}: bed porosity at the minimum of fluidization

According to LEVA, for brut sand, the ratio $\frac{\psi_{mf}^3 \cdot \varphi^2}{1-\psi_{mf}}$ is equals to 0,1 for a mean diameter of approximately 200 μm. Such an estimation can reasonably used for our application. The results are confirmed by the determination of the Reynolds number using the correlation of Thonglimp and Coll:

$$Re_{mf} = (31{,}6^2 + 0.0421 \cdot Ga)^{0.5} - 31.6$$

Ga: Galilée number = $\frac{g \cdot d_p^3 \cdot \rho_f \cdot (\rho_p - \rho_f)}{\mu_f^2}$

The Reynolds numbers found by this correlation and deduced from the determination of U_{mf} are really closed.

The diameter of the particle taken into account (d_p = 100 μm) is the one of the first representative fraction (>5%) of the powder size distribution. We can notice that this diameter corresponds to the particles before processing. Indeed, processing induces attrition of the particles which results in a reduction of the "mean particle diameter". A diminution of the attrition phenomenon is expected with the helicoïdal screw used at a lower velocity.

	Mol. Mass ($kg.mol^{-1}$)	Mol. Diameter (m)	T (°K)	density ($mol.L^{-1}$)	density ($kg.m^{-3}$)	Heat capacity ($J.mol^{-1}.K^{-1}$)	Heat capacity ($kJ.kg^{-1}.K^{-1}$)	Viscosity (10^{-6} Pa.s)	conductivity ($W.m^{-1}.K^{-1}$)	Prandtl
Argon	$39,948.10^{-3}$	$3,40.10^{-10}$ [A]	400	0,03	0,84	29,2	1,042	22,2	0,0323	0,716
			500	0,024	0,67	29,6	1,057	26,1	0,0385	0,716
			600	0,02	0,56	30,1	1,074	29,5	0,0445	0,712
			700	0,017	0,48	30,7	1,096	32,8	0,0505	0,712
Nitrogen	$28,014.10^{-3}$	$3,68.10^{-10}$ [B]	400	0,030	1,201	20,786	0,520	28,8	0,0226	0,663
			473	0,025	1,008	20,786	0,520	32,4	0,0261	0,663
			500	0,024	0,952	20,786	0,520	34,2	0,0268	0,664
			523	0,023	0,910	20,786	0,520	35,5	0,02855	0,663
			548	0,022	0,868	20,786	0,520	37,0	0,0298	0,663
			573	0,021	0,829	20,786	0,520	38,6	0,03105	0,663
			600	0,020	0,791	20,786	0,520	39	0,0306	0,663
Helium	$4,0026.10^{-3}$	$2.58.10^{-10}$ [B]	400	0,03	0,840	20,8	5,197	24,29	0,18433	0,685
			500	0,024	0,672	20,8	5,197	28,36	0,21216	0,695
			573	0,021	0,588	20,8	5,197	31,1379	0,23241	0,696
			600	0,02	0,560	20,8	5,197	32,22	0,23989	0,698
			700	0,017	0,476	20,8	5,197	35,89	0,26751	0,697

Table 8: Thermal properties of Argon, Nitrogen and Helium between 400 and 700 K at 1 bar

The data for Helium and Nitrogen are quoted from the Handbook of Chemistry and physics and the one for the Argon comes from [35].

[A] http://reizei.t.u-tokyo.ac.jp/~maruyama/papers/03/Choi_JKPS2.pdf

[B] www.ornl.gov/sci/fossil/ Publications/ANNUAL-2003/imtl.pdf

Appendix 3

Basic notions in heat transfer

Introduction

Radiation

Conduction

Convection

1 Introduction

Heat transfer occurs between two points at different temperatures. Three ways of transmission exists: by conduction, convection and radiation. The basic equation used in Heat Transfer in steady state is the Newton's law:

$$Q = U \cdot A \cdot \Delta\theta \qquad (1)$$

Q: heat flow (W)
A: heat exchange area (m^2)
$\Delta\theta$: difference of temperature between the two points (°K)
U: overall heat transfer coefficient ($W.m^{-2}.K^{-1}$)

2 Radiation

The radiation is the way of transmission whereby heat flows through a body at a higher temperature to another body at a lower temperature via a transparent environment as air or vacuum.

The heat gives out by an ideal surface called the "black body" is:

$$Q = \sigma \cdot A \cdot T^4 \qquad (2)$$

σ: universal constant of Stephan Boltzman = $5.66697.10^{-8}$ $W.m^{-2}.K^{-4}$
A: surface of the black body
T: temperature of the surface

For an ordinary body, the heat gives out is equal to $\sigma \cdot \varepsilon \cdot A \cdot T^4$ with ε the emissivity or the absorptance of the body. When a body 1 gives out $\sigma \cdot \varepsilon_1 \cdot A_1 \cdot T_1^4$ to another body 2, 2 gives in $\sigma \cdot \varepsilon_1 \cdot \varepsilon_2 \cdot A_1 \cdot T_1^4$. The problems of radiation are quite complex. In the pilot, heat by radiation is indirectly taken into account in the calculation of the effective thermal conductivity (appendix 6)

3 Conduction

The conduction is the way of transmission involved by the difference of temperature between two regions of a solid, a gas or a liquid and between two environments in contact. This phenomenon is a consequence of the movement of molecules and electrons. The fundamental law of the conduction is due to Fourier in one dimension:

$$Q = -k \cdot A \cdot \frac{dt}{dx} \qquad (3)$$

$\frac{dt}{dx}$: temperature gradient at the point x = the temperature variation per length unity in the direction x
A: normal surface of the heat exchange (m^2)
k: thermal conductivity of the material ($W.m^{-1}.K^{-1}$)

k depends on the chemical nature of the material, the nature of the phase (solid, liquid and gas), the temperature, and the orientation in anisotropic materials. In the process, the oxidation and carbonation occurred at a steady state; consequently we will consider k as constant for a

given material. Moreover, the materials used are isotropic.

In steady state conditions, integration of (1) leads to the heat transfer through a plane and a cylinder of thermal conductivities k:

$$Q = -k \cdot A \cdot \frac{\theta_L - \theta_0}{L} \qquad (4)$$

$$Q = -2 \cdot \pi \cdot k \cdot L \frac{\theta_{int} - \theta_{ext}}{\ln \frac{r_{int}}{r_{ext}}} \qquad (5)$$

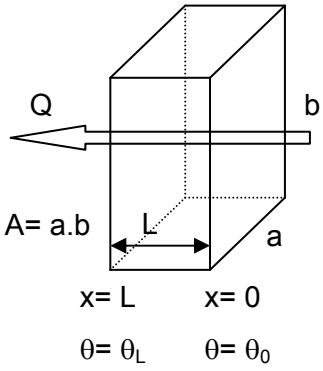

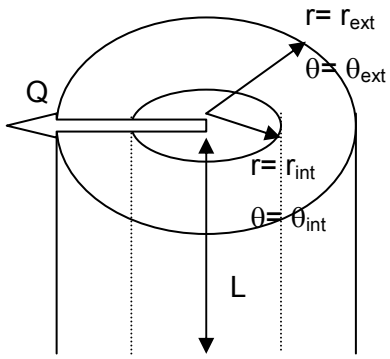

4 Convection

The convection is a way of transmission which implies the displacement of a fluid. It is involved in the heat exchange between a wall and a fluid. In reality, it corresponds to an association between phenomena of conduction and mass transfer. The heat is exchanged by conduction but the movement of the fluid allows mixing the particles responsible of the transfer. Between brackets, in the case of a granular bed in movement, an analogy is possible considering this one as a quasi-homogeneous environment. Thus, the heat is transferred by conduction and the agitation allows by the mixing of the particles to increase the heat transfer rate. Some authors speak about a “convective mix effect”.

Two kinds of convection are distinguished: the forced convection in which the movement of the fluid is due to any device (pump or ventilator for example) and the natural convection due only to the difference of density induced by the difference of temperature within the fluid. Of course, in an industrial installation, forced convection is mainly brought into play.

The global phenomenon of convection between a surface and the fluid which flows around is expressed as:

$$Q = h \cdot A \cdot (T_s - T_\infty) \qquad (6)$$

h: the convection coefficient ($W.m^{-2}.K^{-1}$)
A: the section of heat exchange normal of the heat flow between the surface and the fluid (m^2)
T_s: the temperature of the surface (K)
T_∞: the temperature of the fluid far from the surface (K)

The problem of convection often consists of the resolution of some empirical correlations in dimensionless form to determine the Nusselt number and then h.

- Forced convection

Depending on the regime of the flow, several correlations are available to estimate the Nusselt number for forced convection in a cylindrical pipe.

For a laminar regime with a Reynolds number (Re) lower than 2100:

$$Nu = 1{,}86 \cdot \sqrt[3]{Re \cdot Pr} \cdot \sqrt[3]{\frac{D}{L}} \cdot \left(\frac{\mu}{\mu_p} \right) \qquad (7)$$

Re: Reynolds number (see the last point)
Pr: Prandtl number (see the last point)
D: diameter of the tube (m)
L: length of the tube (m)
μ: dynamic viscosity of the fluid (Pa.s), the subscript p means: near the wall

This correlation is available for $\frac{Re \cdot Pr.D}{L} \geq 12$

For the turbulent and transitional regimes with Re higher than 2300, the Petukhov-Gnielensky correlation is:

$$Nu = \frac{\xi/8 \cdot (Re - 1000) \cdot Pr}{1 + 12.7 \cdot \sqrt{\xi/8} \cdot (Pr^{2/3} - 1)} \cdot \left(1 + \left(\frac{D}{L} \right)^{2/3} \right) \qquad (8)$$

$$\xi = \frac{1}{(1.82 * \log(Re) - 1.64)^2}$$

This correlation is available for $0{,}5 < Pr < 10^6$

In these equations the temperature and the properties of the fluids are taken at the arithmetic average temperature between inlet and outlet.

- Natural convection

The correlations which deal with natural convection are useful for the estimation of the convection coefficient between a reactor and the ambient air in order to calculate the heat loss.

All the correlations have the same form:

$$Nu = C \cdot (Pr \cdot Gr)^n \qquad (9)$$

Gr: Grashof number
C and n two numbers which depends on the surface and of the regime

Below are presented the values of n and C for the practical cases involved with the reactor MSR:

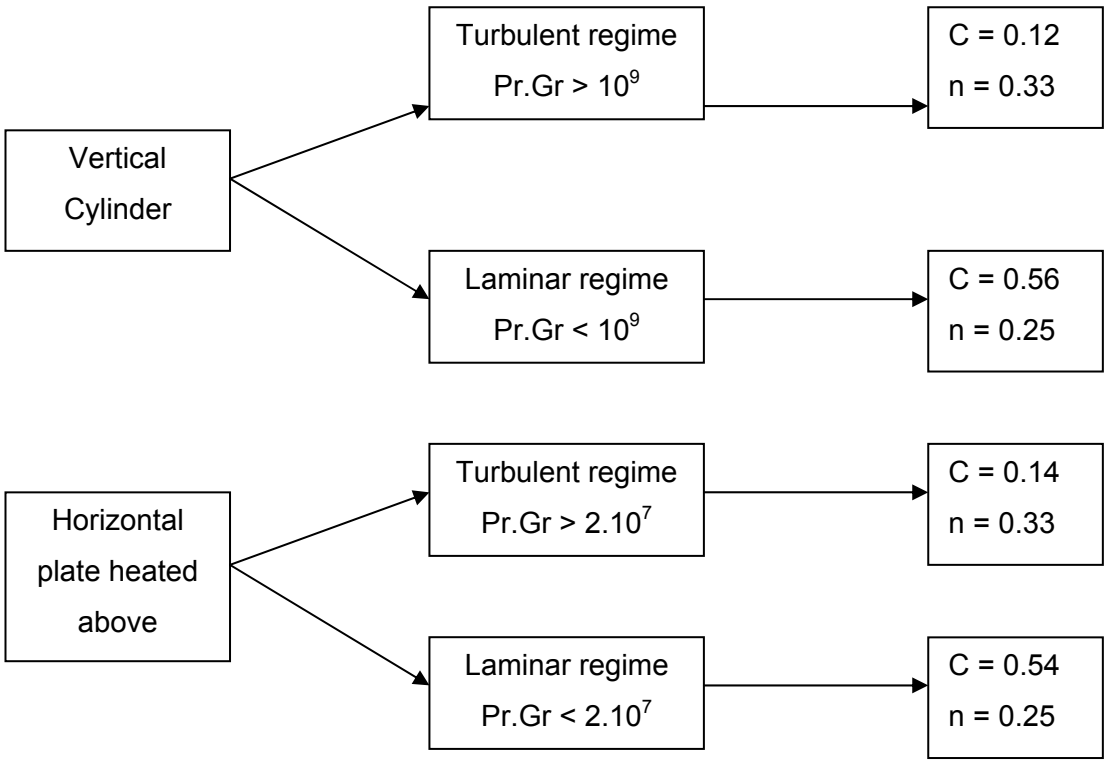

- As shows it the correlations above, several dimensionless groups are useful in convection.

A brief review is given there:

Reynolds's number: $Re = \frac{D \cdot U \cdot \rho_f}{\mu_f}$

Prandtl number: $Pr = \frac{Cp_f \cdot \mu_f}{k_f}$

Nusselt number: $Nu = \frac{h \cdot D}{k_f}$

Peclet number: $Pe = \frac{\rho_f \cdot U \cdot D \cdot Cp_f}{k_f} = Pr \cdot Re$

Grashof number: $Gr = \frac{\beta \cdot g \cdot \Delta\theta \cdot \rho_f^2 \cdot L^3}{\mu_f^2}$

With:
U: axial velocity of the fluid ($m.s^{-1}$)
ρ_f: density of the fluid ($kg.m^{-3}$)
μ_f: dynamic viscosity of the fluid (Pa.s)
Cp_f: heat capacity of the fluid ($j.kg^{-1}.K^{-1}$)
k_f: thermal conductivity of the fluid ($W.m^{-1}.K^{-1}$)
D: diameter of the tube where the fluid is flowing(m)

g: gravity acceleration = 9.81 $m.s^{-2}$

β: thermal expansion (K^{-1}). For a perfect gas: $\beta = 1/T_f$

T_f: temperature of the fluid (K)
T_{wall}: temperature of the wall (K)
$\Delta\theta = T_{wall}-T_f$ (K)
L: In natural convection, mean dimension of the surface (m):

- the diameter for a cylinder
- the width for a plane surface

N-B: In the case of a fluid flowing outside a tube and in parallel, D must be replaced by an equivalent diameter (D_{eq})

$$D_{eq} = 4 * \frac{S}{P}$$

S: bypass section (m^2)
P: wet circumference (m)

N-B: In the case of biphasic system such as furnished column or packed bed, a reduced Reynolds number is often used taking into account the mean diameter of the particles ($\bar{d}_s$).

$$Re_p = \frac{\bar{d}_s \cdot U \cdot \rho_f}{\mu_f}$$

Appendix 4

The heat loss in the reactor MSR

The heat loss occurs between the double mantle and the ambient air through the insulation of the reactor. Consequently, the three phenomena of transmission bring into play are:

- forced convection in the double mantle (h)
- the conduction through the insulation (K)
- natural convection in the vicinity of the reactor (h_{cyl} and h_{plate})

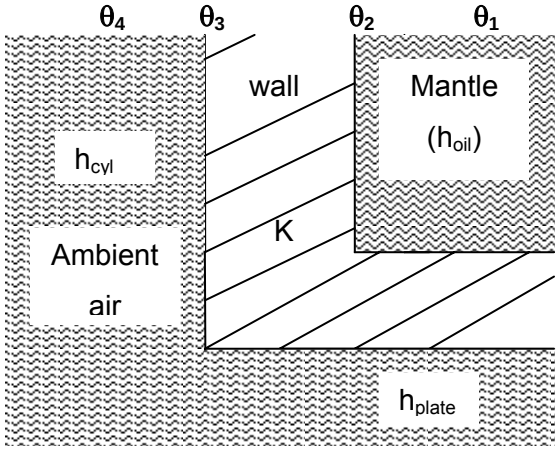

Between the coolant and the wall:

$$Q = h_{oil} \cdot A_{ins} \cdot (\theta_1 - \theta_2) \quad (1)$$

In the wall:

$$Q = K \cdot (\theta_2 - \theta_3) \quad (2)$$

Between the air and the extern wall:

$$Q = (h_{cyl} \cdot A_{cyl} + h_{plate} \cdot A_{plate}) \cdot (\theta_3 - \theta_4) \quad (3)$$

Q: heat loss (W)
A_{ins}: effective surface of contact between the coolant and the insulation (m^2) (appendix 2, table 3)
A_{cyl}: heat exchange area between air and the insulation cylinder (m^2) (appendix 2, table 3)
A_{plate}: heat exchange area between air and the bottom of the insulation (m^2) (appendix 2, table 3)
h_{oil}: convection coefficient of the coolant ($W.m^{-2}.k^{-1}$)
h_{cyl}: convection coefficient of the ambient air in the vicinity of the insulation cylinder ($W.m^{-2}.k^{-1}$)
h_{plate}: convection coefficient of the ambient air in the vicinity of the insulation bottom ($W.m^{-2}.k^{-1}$)

As the coefficient of natural convection depends on the nature of the surface (appendix 3), the heat transfer is break up in two contributions in the vicinity of the insulation cylinder and in the vicinity of the insulation bottom. The two coefficients h_{plate} and h_{cyl} are calculated with the correlations presented in appendix 3. The temperature of the ambient air is taken at 30 °C. The temperature of the extern wall is also needed (θ_4). Consequently, a temperature of 270°C equals at the coolant temperature has been assumed at the beginning as the maximal temperature of the extern wall. Then an iterative calculation has been achieved. Indeed, with such assumption, a first estimation of Q could be done. Then, according to the equation (3) above, it is possible to calculate the temperature of the wall. With this new temperature of the wall, h_{plate} and h_{cyl} are re-estimated, etc…

h_{oil} is calculated in the section 5.4.

The heat transferred by conduction in the bed is the sum of two contributions: the heat exchanged by the insulation cylinder and the heat exchanged by the bottom of the insulation.

According to the section related of the conduction in appendix 3:

$$K = k_{insulation} \cdot \left(\frac{2 \cdot \pi \cdot L_{mantle}}{\ln\left(D_{ext} / D_{int} \right)} + \frac{A_{plate}}{t_{insulation}} \right) \quad (4), \text{ with:}$$

$k_{insulation}$: conductivity of the wall = 0.064 $W.m^{-1}.k^{-1}$
D_{ext}: external diameter of the insulation (m)
D_{int}: internal diameter of the insulation (m)
t_{ins}: thickness of the insulation (m)
All the data linked to these parameters are presented in appendix 2.

Isolating the three differences of temperature for relations (1) to (3) and doing the sum of each one leads finally to:

$$\theta_1 - \theta_4 = Q \left(\frac{1}{h_{oil} \cdot A_{ins}} + \frac{1}{h_{cyl} \cdot A_{cyl} + h_{plate} \cdot A_{plate}} + \frac{1}{k_{insulation} \left(\frac{2 \cdot \pi \cdot L_{mantle}}{\ln\left(D_{ext} / D_{int} \right)} + \frac{A_{plate}}{t_{insulation}} \right)} \right) \quad (5)$$

Thus, it is possible to express the heat flux Q in function of the difference of temperature between the ambient air (at 30°C) and the coolant (270°C). The final results are presented below:

Q = 274 W

U.A = 1.14 $W.K^{-1}$

T_{wall} = 64°C

h_{cyl} = 5.5 $W.m^{-2}.K^{-1}$

h_{plate} = 6.4 $W.m^{-2}.K^{-1}$

Appendix 5

The size distribution of the bed

The size distribution of the bed has been determined by sieve. Two different samples have been tested with different apertures:

- The granular bed before the conversion
- The granular bed after the conversion

The results are presented below:

Sieve aperture diameter (μm)	Mean equivalent diameter (μm)	Mass percentage (%)	
		Before proces.	After proces.
>425	425	13,6	11,8
355-425	390	6,1	
300-355	322.5	12,0	13,0
250-300	275	16,5	
212-250	231	14,1	27,5
180-212	196	14,8	
150-180	165	7,5	
125-150	237.5	6,0	11,4
90-125	107.5	5,2	8,6
53-90	71.5	2,3	3,5
20-53	36.5	0	19,5
<20	20	0,2	4,4

Table1: Size distribution of the matrix after and before processing

It appears that the conversion causes a reduction of the diameter of the particles. Two reasons could be evoked, the main one is that we use scrappers at very high velocity which could induce the attrition of the particles. The first chart shows a displacement of the cumulative size distribution toward the lower diameters. Moreover, the second chart highlights a new distribution with two majority fractions at really different sizes (between 20 and 53 and between 150 and 250 μm). This is maybe due to the formation of new particles induced by the conversion of the sodium in sodium carbonate.

Nevertheless, attrition seems to be the main cause of this diminution. However, with the new stirring device more adapted to the granular systems and with a low velocity, attrition will be normally less important. That will be of a great interest to determine the new size distribution after a conversion with the new system.

			Before processing	After processing
mass average diameter	$\overline{d}_w$	μm	255	172
volume surface mean diameter	$\overline{d}_S$	μm	216	155
coef. of variation of the distribution	ξ_r		0,71	1
distribution function	$f(\xi_r)$		3,12	4,1

Table 2: Mean properties of the distribution before and after processing

ξ_r and $f(\xi_r)$ are defined in appendix 6 whereas $\overline{d}_w$ and $\overline{d}_S$ are defined below:

$$\overline{d}_w = \sum_{i=1}^{n} x_i \cdot \overline{d}_{pi} \quad \text{and} \quad \overline{d}_S = \frac{1}{\sum_{i=1}^{n} x_i / \overline{d}_{pi}} \qquad \text{where:}$$

x_i : mass fraction in a given increment,

$\overline{d}_{pi}$ = average diameter, taken as the arithmetic average of the smallest and largest particle diameters in increment.

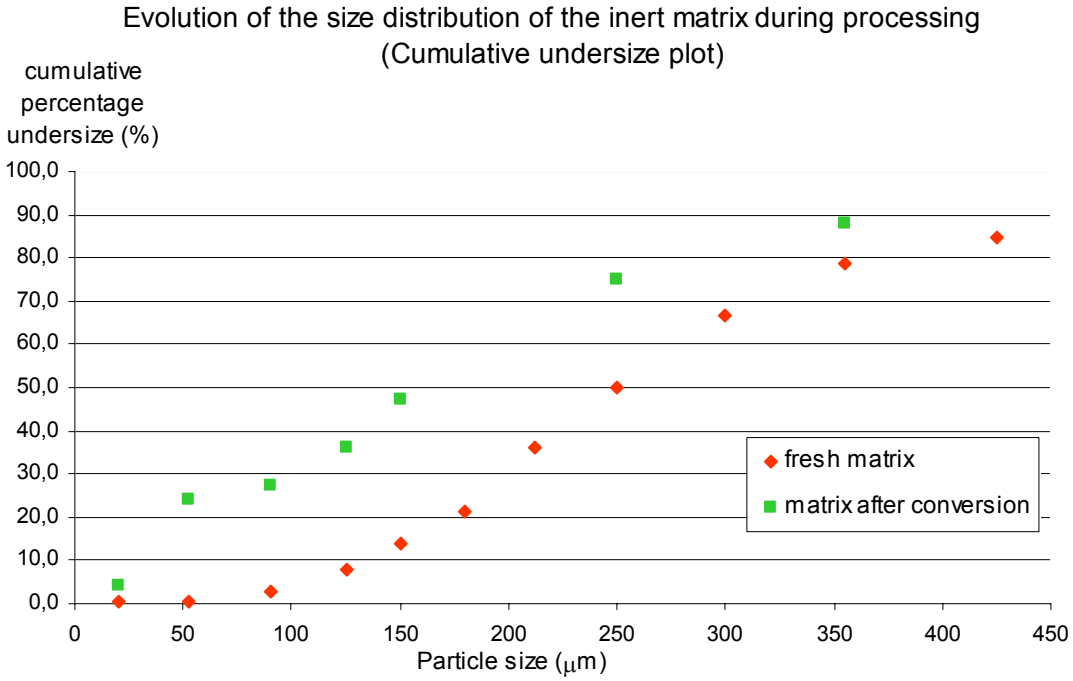

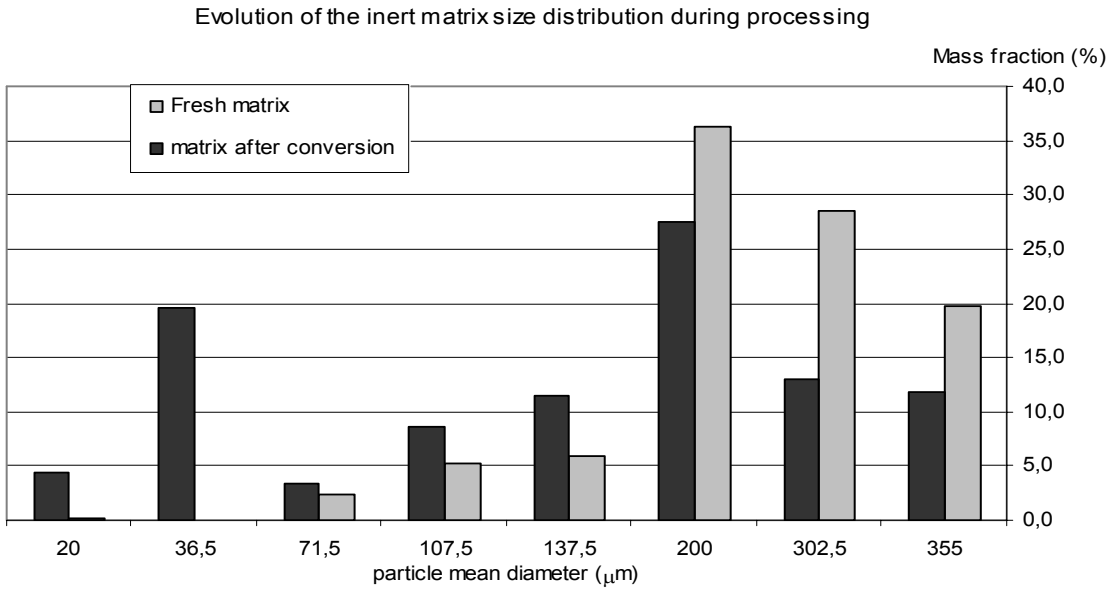

Appendix 6

Determination of the effective thermal conductivity for a broken solid

1 Introduction

As it is explained in the section 4.2, the effective radial conductivity of a bed in a gas flow (k_{bed}) is the sum of two contributions. In a dimensionless relation:

$$\frac{k_{bed}}{k_{gas}} = \left(\frac{k_{bed}}{k_{gas}}\right)_{convection} + \left(\frac{k_{bed}}{k_{gas}}\right)_{\substack{conduction \\ radiation}} \quad (1)$$

2 The convective lateral mixing

The first contribution is due to the convective lateral mixing of the flow [21, part I]:

$$\left(\frac{k_{bed}}{k_{gas}}\right)_{convection} = \frac{Pe_x}{K} = \frac{m_o Cp_{gas}}{k_{gas}} \cdot \frac{x_F}{K} \quad (2)$$

Pe_x: Peclet number formed with a mixing length x_F where convection transfer occurs
m_o: mass flow rate of the gas ($kg.m^{-2}.s^{-1}$)
Cp_{gas}: heat capacity of the gas ($J.kg^{-1}.K^{-1}$)
k_{gas}: thermal conductivity of the gas ($W.m^{-1}.K^{-1}$)
K: a constant depending on the ratio between the bed and the particles diameters

$$K = 8 \cdot \left[2 - \left(1 - \frac{2}{d_{bed}/\overline{d}}\right)^2\right] \quad (3)$$

$\overline{d}$: mean particle size (see appendix 5)

$$x_F = F \cdot \overline{d}$$

For a broken solids, F≈1,55

3 The conductive and radiative contribution

The second contribution is due to the combined conduction and radiation exchanges [21,Part II]

$$\left(\frac{k_{bed}}{k_{gas}}\right)_{\substack{conduction \\ radiation}} = \left(1 - \sqrt{1-\psi}\right) \cdot \left[\frac{\psi}{(\psi - 1) + \frac{k_{gas}}{k_D}} + \psi \frac{k_R}{k_{gas}}\right] + \sqrt{1-\psi} \cdot \left[\varphi \frac{k_S}{k_{gas}} + (1-\varphi)\frac{k^*_{bed}}{k_{gas}}\right] \quad (4)$$

ψ: porosity of the bed
φ: fraction of the heat transfer due to possible contact surfaces between particles
ρ_K^2 : contact area of the solid path related to the projected particle area (m^2)

$$\varphi = \frac{23\rho_K^2}{1 + 22\rho_K^{4/3}} \quad (5)$$

The authors found ρ_K^2 = 0,001 for the sand. We will use this value. It has not a strong influence as this parameter becomes only important at low pressure [12].

- k_S: mean thermal conductivity of the solid phase ($W.m^{-1}.K^{-1}$)

In the case of particles covered with a layer of a substance, a modified k_s should be used:

$$k_s^* = k_s \left(\frac{1}{1 + s_{ox} \cdot k_s / k_{ox} \cdot \bar{d}} \right) \quad (6)$$

s_{ox}: thickness of the layer (m)
k_{ox}: thermal conductivity of the layer ($W.m^{-1}.K^{-1}$)

- k_R is the equivalent conductivities between the surfaces of the solid phase due to thermal radiation ($W.m^{-1}.K^{-1}$):

$$\frac{k_R}{k_{gas}} = \frac{0{,}04 C_s}{(2/\varepsilon - 1) \cdot k_{gas}} \left(\frac{T_{bed}}{100} \right)^3 \cdot x_R \quad (7)$$

ε: emissivity of the particles
C_s: Stephan-Boltzmann constant = $5{,}67.10^{-8}$ $W.m^{-2}.K^{-4}$
T_{bed}: temperature of the bed (K)
x_R : effective radiation length that characterizes the distance between the particle surfaces of any packing and must take into account the geometry of these surfaces (m)

$$x_R = R \cdot \bar{d}$$

For a broken solid, R ≈ 1

- k_D is the equivalent conductivities between the surfaces of the solid phase due to Smoluchowski effect ($W.m^{-1}.K^{-1}$):

$$\frac{k}{k_D} = 1 + \frac{2\sigma}{x_D} \left(\frac{2}{\gamma} - 1 \right) \quad (8)$$

x_D : effective gas path that characterizes the size of the vapour space between the particles (m)
γ: accommodation coefficient [10]
σ: mean free path of the gas molecules (m)

$$x_D = D \cdot \bar{d}$$

D has been not found yet for a broken solid, nevertheless, D ≈ 1 for a sphere. This value will be chosen for the sodium carbonate. A value close of 1 is expected as the effective gas path for a broken solid should be close than the gas path of a sphere. Simulations show that changing this value from 0.8 to 3 implies no variation at two digits after the coma.

γ depends on the nature and the temperature of the gas:

$$\log\left(\frac{1}{\gamma} - 1 \right) = 0{,}6 - \left[\frac{1000}{T} + 1 \right] \frac{1}{C}$$

C = 2,8 for Air, 3 for Argon and 50 for helium

$$\sigma = \frac{R.T}{\sqrt{2}\cdot P\cdot \pi \cdot N_A \cdot d_{mol}^2} = \frac{8{,}4\cdot 10^{-27}}{d_{mol}^2}\left(\frac{T}{273.15}\right)\left(\frac{101300}{P}\right) \qquad (9)$$

N_A: Avogadro's number = $6{,}02.10^{23}$ mol^{-1}
R: Gas constant = 8.314 $J.K^{-1}.mol^{-1}$
P: gas pressure (Pa)
T: gas temperature (K)
d_{mol}: molecular diameter (m)

- k^*_{bed} corresponds to the transfer through two particle halves that are separated by a wedge of gas ($W.m^{-1}.K^{-1}$):

$$\frac{k^*_{bed}}{k_{gas}} = \frac{2}{K}\cdot\left\{\begin{array}{l} \dfrac{B\left(\dfrac{k_S}{k_{gas}}+\dfrac{k_R}{k_{gas}}-1\right)\dfrac{k_{gas}}{k_D}\Big/\dfrac{k_S}{k_{gas}}}{K^2}\cdot \ln\dfrac{\left(\dfrac{k_S}{k_{gas}}+\dfrac{k_R}{k_{gas}}\right)\cdot\dfrac{k_{gas}}{k_D}}{B\left[1+\left(\dfrac{k_{gas}}{k_D}-1\right)\left(\dfrac{k_S}{k_{gas}}+\dfrac{k_R}{k_{gas}}\right)\right]} \\ -\dfrac{B-1}{K}\dfrac{k_{gas}}{k_D}+\dfrac{B+1}{2B}\left[\dfrac{k_R}{k_{gas}}\dfrac{k_{gas}}{k_D}-B\left(1+\left(\dfrac{k_{gas}}{k_D}-1\right)\dfrac{k_R}{k_{gas}}\right)\right] \end{array}\right\} \qquad (10)$$

With :

$$K = \left[1+\left(\frac{k_R}{k_{gas}}-B\Big/\frac{k_{gas}}{k_D}\right)\Big/\frac{k_s}{k_{gas}}\right]\frac{k_{gas}}{k_D}-B\left(\frac{k_{gas}}{k_D}-1\right)\left(1+\frac{k_R}{k_{gas}}\Big/\frac{k_s}{k_{gas}}\right) \qquad (11)$$

B is a parameter which formulates the influence of the particle size distribution, the particle's shape and the porosity:

$$B = C_{form}\cdot\left(\frac{1-\psi}{\psi}\right)^{10/9} f(\xi_r) \qquad (12)$$

For a broken solid, $C_{form} \approx 1.4$

$f(\xi_r)$ is a distribution function

$$f(\xi_r) = 1 + 3\xi_r \qquad (13)$$

ξ_r is the coefficient of variation of the numerical distribution:

$$\xi_r = \left[\frac{\sum_{i=1}^{n} x_i / d_{pi}^2}{\left(\sum_{i=1}^{n} x_i / d_{pi}\right)^2} - 1\right]^{1/2} \qquad (14)$$

x_i : mass fraction in a given increment
$\overline{d}_{pi}$ = average diameter, taken as arithmetic average of the smallest and largest particle diameters in increment.

Appendix 7

Influence of various variables on the heat transfer coefficient in the bed

Influence of the efficiency of the mixer

Influence of the “wall surface-to-bed surface” heat transfer coefficient

Influence of the effective thermal conductivity

Simulations have been done in order to show the influence of the three main parameters required on the estimation of the heat exchange coefficient between the bed and the wall (α).

- Influence of the mixing number (N_{mix})

As N_{mix} has not been determined yet, the value taken in consideration in the rapport are assumed according to values taken from the literature for similar devices. The chart below shows the influence of this number.

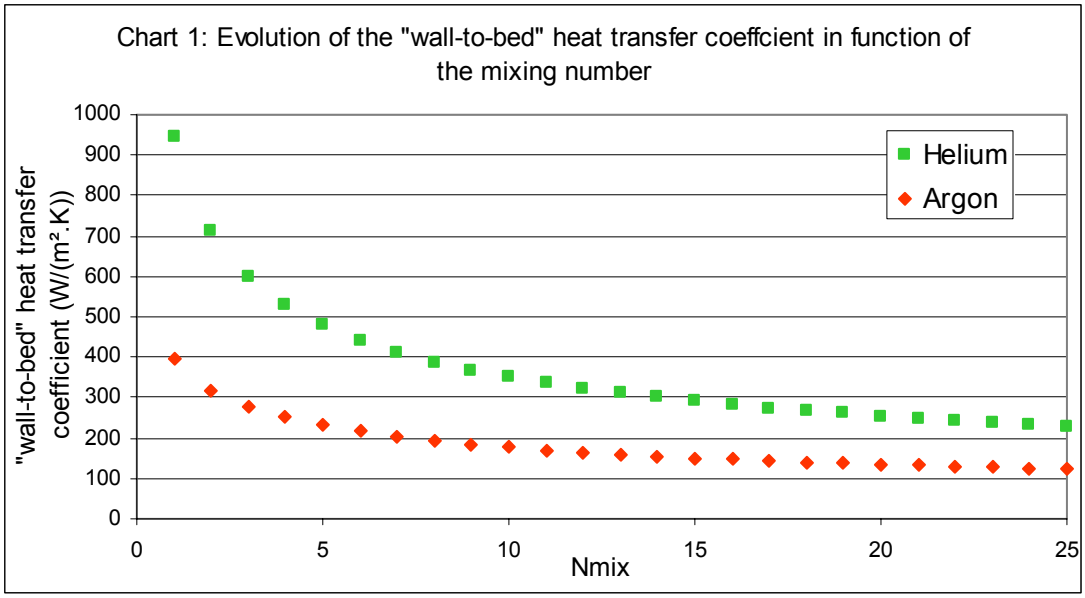

In the literature, the values found for N_{mix} vary from 1 to 25. This chart has been constructed considering an agitation velocity of 165 rpm and the other parameters used in the chapter 5.

For the low values of N_{mix}, α is strongly affected which shows the importance of a good estimation of this parameter in the future.

- Influence of the “wall surface-to-bed surface” heat transfer coefficient (α_{WS})

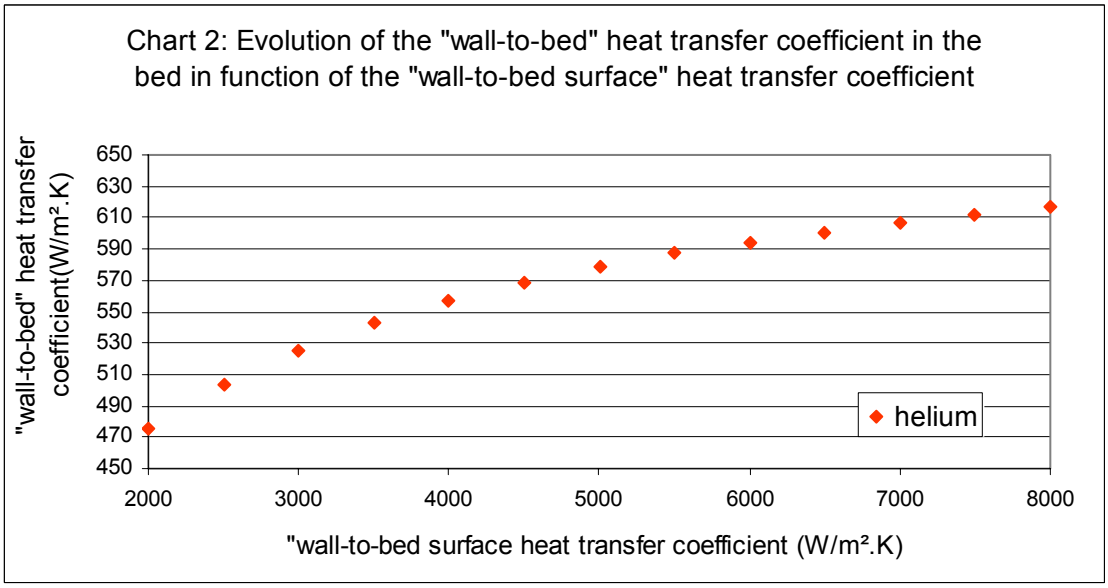

Due to the fact that the roughness size (δ) and the true temperature of the gas in the void fraction (t_{gas}) are not exactly known, this coefficient is not estimated with a satisfying accuracy. The chart above shows that the dependence is not so strong in the case of helium as interstitial gas, with a velocity of 165 rpm and an efficiency of 3. Indeed, considering the worst conditions (δ = 1 μm and T_{gas} = 200°C) leads to a coefficient of approximately 6200 $W.m^{-2}.K^{-1}$. On the contrary, if we consider the best conditions (δ = 0 μm, T_{gas} = 300°C), α_{WS} is more or less equals to 7000. Finally, the variation of α is approximately lower than 5 %.

- Influence of the effective thermal conductivity

As the effective thermal conductivity (k_{bed}) of the bed is estimated according to a model, the value used in the calculation is maybe a little bit different of the real one. This chart shows its influence on the heat transfer coefficient in the bed.

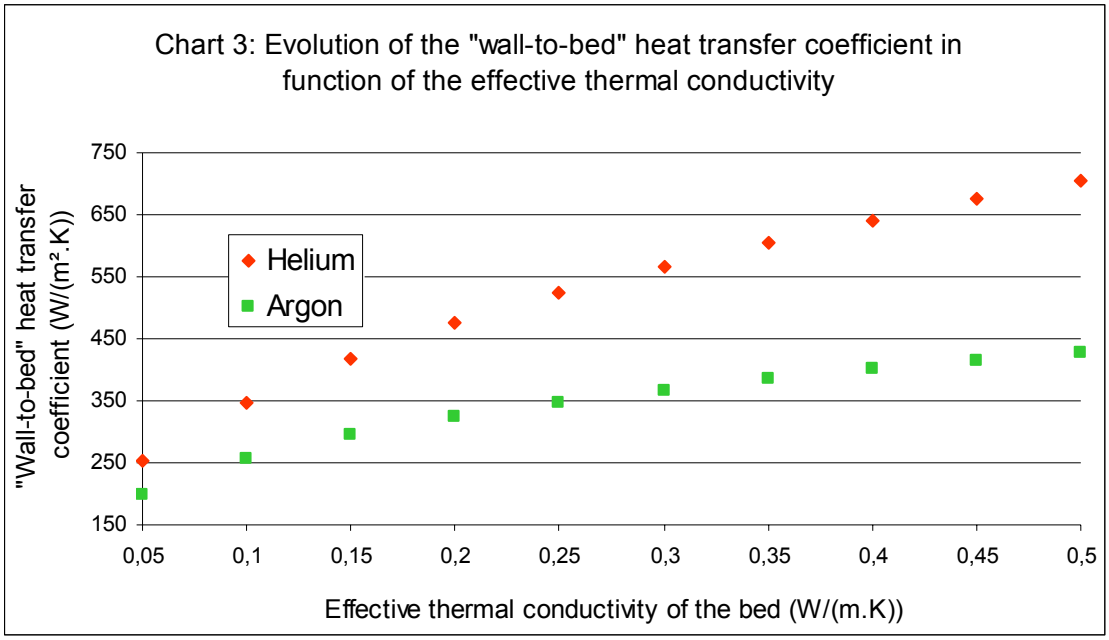

A mixing number equals to 3 is assumed at 165 rpm in this simulation.

It appears that the heat transfer coefficient quite strongly depends of k_{bed}. Nevertheless, in the most practical cases, k_{bed} is included between the true thermal conductivity of the gas and the particles. Consequently, in the case of a flow of helium, k_{bed} may be located between 0.25 and 0.5 $W.m^{-1}.K^{-1}$, leading to a heat transfer coefficient between 550 and 700 $W.m^{-1}.K^{-1}$.

- Conclusion

A lot of parameters are taken into account for the calculation of the heat exchange coefficient which makes impossible an accurate value of it. Nevertheless, according to the different simulation, it may be possible to estimate an order of magnitude with a quite good accuracy. In this study, this coefficient is maybe a little bit underestimated as the worst conditions have been always chosen.